

1 **Continental pollution in the Western Mediterranean basin: vertical profiles of**  
2 **aerosol and trace gases measured over the sea during TRAQA 2012 and**  
3 **SAFMED 2013**

4 C. Di Biagio<sup>1</sup>, L. Doppler<sup>2,3,4</sup>, C. Gaimoz<sup>1</sup>, N. Grand<sup>1</sup>, G. Ancellet<sup>2</sup>, J.-C. Raut<sup>2</sup>, M. Beekmann<sup>1</sup>, A.  
5 Borbon<sup>1</sup>, K. Sartelet<sup>5</sup>, J.-L. Attié<sup>6,7</sup>, F. Ravetta<sup>2</sup>, and P. Formenti<sup>1</sup>

6 (\*corresponding author: claudia.dibiagio@lisa.u-pec.fr)

7  
8 <sup>1</sup> *LISA, UMR CNRS 7583, Université Paris Est Créteil et Université Paris Diderot, Institut Pierre*

9 *Simon Laplace, Créteil, France*

10 <sup>2</sup> *Sorbonne Universités, UPMC Univ. Paris 06; Université Versailles St-Quentin; CNRS/INSU,*

11 *LATMOS-IPSL, Paris, France*

12 <sup>3</sup> *Freie Universität Berlin, Berlin, Germany*

13 <sup>4</sup> *Deutscher Wetterdienst, Meteorological Observatory Lindenberg, Germany*

14 <sup>5</sup> *CEREA, Joint Laboratory École des Ponts ParisTech – EDF R & D, Université Paris-Est, 77455*

15 *Marne la Vallée, France*

16 <sup>6</sup> *Laboratoire d'Aérodologie, University of Toulouse, UMR 5560 CNRS, France*

17 <sup>7</sup> *CNRM GAME UMR 3589 CNRS, METEO-FRANCE*

18  
19 **Abstract**

20 In this study we present airborne observations of aerosol and trace gases obtained over the sea in the  
21 Western Mediterranean basin during the TRAQA (TRansport and Air QuAlity) and SAFMED  
22 (Secondary Aerosol Formation in the MEDiterranean) campaigns in summers 2012 and 2013. A  
23 total of 23 vertical profiles were measured up to 5000 m above sea level over an extended area

24 (40°-45°N latitude and 2°W-12°E longitude) including the Gulf of Genoa, Southern France, the  
25 Gulf of Lion, and the Spanish coast. During TRAQA and SAFMED the study area experienced a  
26 wide range of meteorological conditions which favoured the pollution export from different sources  
27 located around the basin. Also, several events of dust outflows were measured during the  
28 campaigns. Observations from the present study show that continental pollution largely affects the  
29 Western Mediterranean both close to coastal regions and in the open sea as far as ~250 km from the  
30 coastline. The measured aerosol scattering coefficient varies between ~20 and 120 Mm<sup>-1</sup>, while  
31 carbon monoxide (CO) and ozone (O<sub>3</sub>) mixing ratios are in the range of 60-165 ppbv and 30-85  
32 ppbv, respectively. Pollution reaches 3000-4000 m in altitude and presents a very complex and  
33 highly stratified structure characterized by fresh and aged layers both in the boundary layer and in  
34 the free troposphere. Within pollution plumes the measured particle concentration in the Aitken  
35 (0.004-0.1 μm) and accumulation (0.1-1.0 μm) modes is between ~100 and 5000-6000 scm<sup>-3</sup>  
36 (standard cm<sup>-3</sup>), which is comparable to the aerosol concentration measured in continental areas  
37 under pollution conditions. Additionally, our measurements indicate the presence of highly  
38 concentrated Aitken layers (10000-15000 scm<sup>-3</sup>) observed both close to the surface and in the free  
39 troposphere, possibly linked to the influence of new particle formation (NPF) episodes over the  
40 basin.

41

## 42 **1. Introduction**

43 Atmospheric aerosols play an important role on climate through their participation to several  
44 chemical, dynamical, and radiative processes. At present, still large uncertainties persist in the  
45 estimation of the aerosol direct and indirect effects mainly due to the difficulty of fully  
46 characterizing their spatial and vertical distribution and properties (Boucher et al., 2013).

47 The Mediterranean region is a complex area where atmospheric aerosols of different origins and  
48 types may be found (Pace et al., 2006; Kallos et al., 2007; Gkikas et al., 2012). High levels of

49 anthropogenic aerosol particles and pollutants are measured in the Mediterranean (Lelieveld et al.,  
50 2002), which is also indicated as one of the main hot spots for air quality issues (Monks et al.,  
51 2009).

52 The North-Western part of the Mediterranean basin, due to its proximity to highly polluted  
53 industrialized areas (such as the Po Valley in northern Italy and the Fos/Berre in southern France)  
54 and large coastal cities (Barcelona, Genoa, Marseilles, Nice, or Valencia), is frequently affected by  
55 continental outflows and severe pollution episodes (Mallet et al., 2005; Pérez et al., 2008; Pey et al.,  
56 2010). The strength of these episodes is particularly intense during summer when stable  
57 meteorological conditions and the high level of insolation promote photochemical reactions and the  
58 build-up of ozone and other pollutants (e.g. Millán et al., 2000).

59 A number of studies have investigated the dynamics of pollution export over the Western basin with  
60 the aim of characterizing the impact of anthropogenic emissions over this region. Most of these  
61 studies have been conducted in continental coastal areas and provide information on the vertical  
62 distribution of aerosols and their properties mainly close to local pollution sources. They include  
63 ground-based observations with lidars (Soriano et al., 2001; Pérez et al., 2004; Ancellet and  
64 Ravetta, 2005), and airborne campaigns, such as MECAPIP (MEso-meteorological Cycles of Air  
65 Pollution in the Iberian Peninsula) and RACAPMA (RegionAl Cycles of Air Pollution in the west  
66 central Mediterranean Area) in coastal Spain (Millán et al., 1996 and 1997) and ESCOMPTE  
67 (Experience sur Site pour Contraindre les Modeles de Pollution atmospherique et de Transport  
68 d'Emissions) in Southern France (Drobinski et al., 2007). The results of these studies have  
69 highlighted the important role of pollution in modulating the atmospheric composition in this part  
70 of the basin, as well as the high variability of the aerosol distribution and properties in link to  
71 different export conditions (Flamant and Pelon, 1996; Soriano et al., 2001; Mallet et al., 2005). In  
72 particular, the interaction between synoptic circulation and local dynamics, such as orography and  
73 sea breezes, has been shown to strongly impact the vertical distribution, layering, and aging of

74 particles along coastal regions (e.g. Millan et al., 1997; Gangoiti et al., 2001; Pérez et al., 2004;  
75 Velchev et al., 2011).

76 The capability of reproducing this complexity by air quality models represents a real challenge  
77 (Jimenez et al., 2006; Jiménez-Guerrero et al., 2008), and experimental observations gives a  
78 fundamental support to test the performances of the model outputs over the Western Mediterranean  
79 environment.

80 The large set of observations conducted in the last decades has permitted to acquire a detailed  
81 characterisation of pollution aerosols in the surroundings of the Western basin. However, at the  
82 present time we miss an extensive representation of the mean aerosol load, distribution, and  
83 properties in the whole region, in particular over the remote sea. In addition, there is a significant  
84 lack of observations over some key areas, as for example the Gulf of Genoa, directly under the  
85 influence of the outflow from the highly polluted Po Valley (Velchev et al., 2011).

86 In this study we present measurements of aerosols and trace gas vertical profiles acquired during 24  
87 scientific flights performed with the ATR-42 French research aircraft during the TRAQA  
88 (TRansport and Air QuAlity) and SAFMED (Secondary Aerosol Formation in the MEDiterranean)  
89 campaigns in summers 2012 and 2013 in the framework of the Chemistry-Aerosol Mediterranean  
90 Experiment (CHARMEX, <https://charmex.lsce.ipsl.fr/>). The TRAQA and SAFMED flights  
91 explored an extended region of the Western Mediterranean basin between 40°-45°N latitude and  
92 2°W-12°E longitude including the Gulf of Genoa, Southern France, the Gulf of Lion, and the  
93 Spanish coasts. Measurements were performed over the sea at various distances from the coastline  
94 with lidar and in situ instruments. During TRAQA and SAFMED the Western basin was under  
95 diverse synoptic conditions which led to the occurrence of different pollution export regimes  
96 (Mistral/Tramontane events, outflow from the Po Valley and the Iberian Peninsula) and allowed  
97 sampling atmospheric aerosols of different origin and types.

98 The main objective of the present work is to provide observations of the vertical distribution of  
99 aerosols and trace gases related to the export of anthropogenic pollution at the regional scale of the  
100 Western Mediterranean basin. The detailed knowledge of the vertical structure of the atmosphere is  
101 very important to understand the impact of continental pollution over the basin.

102 The paper is organized as follows: in Sections 2, 3, and 4 we describe the flight trajectories and  
103 strategy during TRAQA and SAFMED, the in situ measurements carried out on board the ATR-42  
104 aircraft, and the meteorological conditions observed during the campaigns. In Sect. 5 we present the  
105 results. The aerosols and trace gases vertical profiles are shown in Sections 5.1 and 5.2. Section 5.3  
106 is dedicated to analyse the variability of the pollution plume composition and atmospheric structure  
107 also in link with the different outflow conditions. Airborne measurements in presence of layers with  
108 high concentrations of fine particles are discussed in Section 5.4. The main conclusions are reported  
109 in Section 6.

110

## 111 **2. Overview over flights**

112 Figure 1 shows the trajectories of the flights performed during the TRAQA (20 June-13 July 2012)  
113 and the SAFMED (24 July-1 August 2013) campaigns. Research flights were performed with the  
114 SAFIRE (Service des Avions Français Instruments pour la Recherche en Environnement,  
115 <http://www.safire.fr/>) tropospheric aircraft ATR-42. The aircraft has a maximum endurance of 4 h.  
116 The flight altitude ranges between a minimum of ~60 m over the sea, to a maximum of ~5000 m  
117 above sea level (a.s.l.). The aircraft was based in Toulouse (43°36'N, 1°26'E, France) during  
118 TRAQA and in Genoa (44°24'N, 8°55'E, Italy) during SAFMED. Twenty-four flights for a total of  
119 ~75 hours of data have been collected. Seventeen of the twenty-four flights presented in the paper  
120 were performed during TRAQA (flight numbers V16 to V32) and 7 during SAFMED (V46 to  
121 V52). All flights were carried out during daytime, when light-induced chemistry favours the  
122 pollution levels. Frequently, two flights per day, with intermediate stops in different airports in

123 Southern France, Corsica, and Sardinia, were performed. The majority of flights were over the sea,  
124 with some exceptions investigating inland areas in Southern France and central Italy. Main  
125 information concerning the TRAQA and SAFMED flights is summarized in Table 1.

126 The general flight strategy consisted in plane flights with lidar observations and vertical  
127 ascents/descents to sound the vertical atmospheric column (from ~60-100 m to 3000-5000 m a.s.l.)  
128 and identify main meteorological and aerosol features, followed by straight levelled runs (SLRs)  
129 within the detected aerosol layers. In this study we focus on vertical profiles data. A total of 23  
130 profiles were acquired in 20-30 minutes each by performing a spiral trajectory ~10-20 km wide.  
131 Fig. 1 also identifies the geographical position of each sounding. As shown in Fig. 1 the profiles  
132 were performed at different distances from the coastline, from a minimum of ~5-10 km for V31 and  
133 V32 to more than ~250 km for V20 and V25, and covered almost all the different sectors of the  
134 Western basin.

135

### 136 **3. Measurements and methods**

137 The basic equipment of the ATR-42 aircraft includes sensors for the measurements of  
138 meteorological parameters (pressure, temperature, relative humidity, wind components), radiative  
139 fluxes (down- and up-welling shortwave and longwave radiation), and carbon monoxide (CO) and  
140 ozone (O<sub>3</sub>) mixing ratios.

141 Aerosol sampling was performed using the AVIRAD system (Formenti et al., 2011). AVIRAD is an  
142 iso-axial and iso-kinetic inlet which, at the normal cruise speed of the ATR-42 (~93 m s<sup>-1</sup>), samples  
143 air at a volumetric flow of ~350 l min<sup>-1</sup>. The 50% passing efficiency of the inlet was tested to be 12  
144 μm diameter. Various sampling lines depart from AVIRAD to connect to different instruments  
145 mounted inside the aircraft cabin: (i) a 3-wavelength nephelometer (TSI Inc., model 3563) for the  
146 measurement of the dry particle volume total scattering ( $\sigma_s$ ) and hemispherical backscattering ( $\sigma_{bs}$ )  
147 coefficients at 450, 550, and 700 nm; (ii) a 7-wavelengths aethalometer (Magee Sci., model AE31)

148 for the measurement of the particle absorption coefficient ( $\sigma_a$ ) at 370, 470, 520, 590, 660, 880, and  
149 950 nm; (iii) an optical particle counter (GRIMM Inc., model 1.129) for the measurement of the  
150 particle number concentration over 32 size classes between 0.3 and 32  $\mu\text{m}$  in diameter; (iv) a  
151 Condensation Particle Counter (CPC, TSI Inc., model 3775) for the measurement of the total  
152 particle number concentration in the diameter range 0.004-3.0  $\mu\text{m}$ ; and (v) 3 lines for aerosol  
153 sampling on filter membranes and a 4-stage cascade impactor (Dekati Inc) to measure the bulk and  
154 size-segregated particle composition. In addition, the ATR-42 was equipped with a Passive Cavity  
155 Aerosol Spectrometer Probe (PCASP, model 100X) optical particle counter for the measurement of  
156 the aerosol number concentration over 31 size classes between 0.1–3.0  $\mu\text{m}$ . The PCASP was  
157 installed outside the cabin on the left side of the aircraft fuselage.

158 In this study we consider measurements of the (i) aerosol scattering coefficient from the  
159 nephelometer, (ii) particle concentration from the CPC and PCASP instruments (GRIMM data are  
160 not considered since they are available only below  $\sim 350$  m during TRAQA), (iii) CO and O<sub>3</sub> trace  
161 gases from the MOZART analyser, and (iv) meteorological parameters from the ATR-42 sensors. A  
162 more detailed description of the nephelometer, CPC, PCASP, and MOZART measurements and  
163 their data analysis is provided in the following sections.

164 The present analysis is based only on measurements obtained in cloud free conditions.

165

### 166 **3.1 Aerosol scattering coefficient**

167 A three-wavelength integrating nephelometer has been used to measure the dry particle volume  
168 total scattering ( $\sigma_s$ ) coefficient at 450, 550, and 700 nm. The sampling flow rate was 30 l min<sup>-1</sup>.  
169 Data were acquired at 6 s resolution during TRAQA and 1 s resolution during SAFMED. The  
170 instrument was calibrated prior each campaign with free-particle air and CO<sub>2</sub> as gases of low and  
171 high known scattering coefficient. Nephelometer measurements have been corrected for angular  
172 truncation and Lambertian non-idealities by applying the formulae by Anderson and Ogren (1998).

173 The measurement uncertainty on  $\sigma_s$  is calculated taking into account for the photon counting, gas  
174 calibration, and angular corrections uncertainties (Anderson et al., 1996; Anderson and Ogreen,  
175 1998). The total uncertainty on  $\sigma_s$  is estimated to be lower than 10% at the three wavelengths.

176 The nephelometer measured the scattering coefficient in dry air conditions. This is due to the  
177 heating of the airflow while entering the aircraft cabin and the temperature in the cavity of the  
178 instrument. The relative humidity measured during the flights inside the nephelometer was <25% in  
179 more than ninety percent of cases, with values up to ~40% occasionally observed at very low  
180 altitudes (<200 m) over the sea surface. A possible underestimation of the scattering coefficient  
181 may thus occur in case of hygroscopic aerosols, especially under high relative humidity conditions  
182 in the atmosphere.

183 The particle scattering Ångström exponent ( $\alpha_s$ ) has been calculated from spectral nephelometer  
184 measurements with a power-law fit of the measured scattering coefficients versus wavelength.

185

### 186 **3.2 Aerosol particle number concentration**

187 The vertical profiles of the total particle number concentration in the Aitken ( $dN_{\text{Aitken}}$ , 0.004-0.1  
188  $\mu\text{m}$ ), accumulation ( $dN_{\text{Acc}}$ , 0.1-1.0  $\mu\text{m}$ ) and coarse ( $dN_{\text{Coarse}}$ , >1.0  $\mu\text{m}$ ) modes have been obtained  
189 by combining CPC and PCASP data. The CPC and the PCASP measured at a sample flow of 1.5  
190 and 0.06  $\text{l min}^{-1}$ , respectively, and with a time resolution of 1 s for the PCASP and 5 s and 1 s for  
191 the CPC during TRAQA and SAFMED, respectively.

192 The PCASP was factory calibrated with monodisperse polystyrene sphere latex (PSL) whose  
193 complex refractive index at the instrument operating wavelengths (632.8 nm) is 1.59-0i. The  
194 measured sphere-equivalent optical diameter has been converted to a sphere-equivalent geometrical  
195 diameter ( $D_g$ ) by taking into account the complex refractive index of the sampled aerosol (Liu and  
196 Daum, 2000). Given that in the very large majority of cases the aerosol sampling during TRAQA



197 and SAFMED was associated to the export of pollution plumes, only pollution aerosols have been  
198 considered for PCASP correction. Note that these data are not optimized for dust or marine aerosol  
199 observations. A large interval of values ( $n \sim 1.50-1.72$ ,  $k \sim 0.001-0.1$  for UV-visible wavelengths) are  
200 reported in the literature for the real and the imaginary parts of the refractive index for  
201 anthropogenic aerosols over Europe (e.g., Ebert et al., 2002 and 2004; Müller et al., 2002; Mallet et  
202 al., 2003 and 2011; Chazette et al., 2005; Raut and Chazette, 2008). For our calculations at 632.8  
203 nm we have fixed the imaginary part of the refractive index to 0.01, thus representing a mean  
204 absorbing aerosol, and then we have varied the real part between its minimum (1.50) and maximum  
205 (1.72) reported value.  $D_g$  is then set at the mean  $\pm$  one standard deviation of the values obtained for  
206 the different values of  $n$ . We assume in these calculations that the refractive index does not vary  
207 with height. After refractive index correction the  $D_g$  range for the PCASP becomes 0.10-4.47  $\mu\text{m}$ ,  
208 with an uncertainty between 1 and 25%. The smallest and the largest size bins of the PCASP, for  
209 which the minimum and maximum edges respectively are not defined, have been excluded from the  
210 datasets, thus reducing the PCASP  $D_g$  range to 0.11-4.17  $\mu\text{m}$ .

211 Once corrected for the refractive index, PCASP data have been combined with those from the CPC  
212 to calculate  $dN_{\text{Aitken}}$ ,  $dN_{\text{Acc}}$ , and  $dN_{\text{Coarse}}$ . Values for  $dN_{\text{Acc}}$  and  $dN_{\text{Coarse}}$  are obtained by integrating  
213 the PCASP number concentrations in the 0.1-1.0  $\mu\text{m}$  and 1.0-4.17  $\mu\text{m}$  ranges, while  $dN_{\text{Aitken}}$  is  
214 estimated as the difference between CPC concentration and the integral of PCASP data between 0.1  
215 and 3.0  $\mu\text{m}$ . The comparison between the PCASP and the GRIMM below 350 m altitude indicates  
216 that the former underestimates by about 50% the aerosol concentration in the range 0.4-1.0  $\mu\text{m}$  (the  
217 accuracy of the GRIMM has been verified by optical closure study against simultaneous aircraft  
218 nephelometer measurements). This is estimated to induce a  $\sim 20\%$  underestimation of the  $dN_{\text{Acc}}$   
219 calculated here. Conversely, the PCASP underestimation in the 0.4-1.0  $\mu\text{m}$  range has almost a  
220 negligible impact on  $dN_{\text{Aitken}}$ .

221 CPC measurements, and so  $dN_{\text{Aitken}}$  data, were not available during SAFMED flights V49, V50, and  
222 part of V51.

223

### 224 **3.3 Trace gases**

225 Carbon monoxide (CO) and ozone (O<sub>3</sub>) mixing ratios were measured by the MOZART instrument  
226 described in detail by Nedélec et al. (2003). CO is a long-lived tracer for air masses influenced by  
227 combustion processes, whereas O<sub>3</sub> in the troposphere is a photochemical product of the oxidation of  
228 CO and volatile organic compounds (VOCs) in the presence of nitrogen oxides (NO<sub>x</sub>). CO and O<sub>3</sub>  
229 are measured at a resolution of 30 s and 4 s, respectively. The nominal uncertainty is ±5% for CO  
230 and ±2% for O<sub>3</sub> (Nedélec et al., 2003). However, a recent airborne intercomparison in May 2014 in  
231 the framework of the French ChemCalInt project and the TGOE European Joint Research Activity  
232 has suggested a greater uncertainty (up to 30%) on CO measurement by MOZART on-board the  
233 ATR-42 (A. Borbon, personal communication, 2015). Trace gas analysis will focus mostly on the  
234 vertical distribution of the  $\Delta O_3/\Delta CO$  ratio rather than absolute concentrations (see section 5.3) and  
235 the uncertainty on CO should not affect data interpretation.

236

### 237 **3.4 STP conversion**

238 In order to compare measurements obtained at different altitudes the data presented here are  
239 reported at standard temperature and pressure (STP) using  $T=293.15$  K and  $p=1013.25$  hPa (NIST,  
240 National Institute of Standards and Technology, values). Hence, the scattering coefficient is scaled  
241 to STP conditions and the particle concentrations are given as particles per standard  $\text{cm}^{-3}$  ( $\text{scm}^{-3}$ ).  
242 For a generic parameter  $x$  measured at the temperature  $T$  and pressure  $p$ , the conversion at STP is  
243 calculated with the formula:

244 
$$x(\text{STP}) = x(T, p) \frac{T}{293.15} \frac{1013.25}{p} \quad (1).$$

245 CO and O<sub>3</sub> do not need to be corrected for STP since the mixing ratio does not depend on  
246 temperature and pressure.

247

### 248 **3.5 Meteorological parameters**

249 The vertical profiles of the pressure (p), the temperature (T), the relative humidity (RH) and the  
250 wind components towards the east and the north (U, V) measured on board the ATR-42 have been  
251 used to analyse the atmospheric structure during flights. Starting from the measured parameters the  
252 potential temperature ( $\theta$ ) has been also calculated as  $\theta = T(p_0/p)^{0.286}$  with  $p_0=1013.2$  mbar. For  
253 each profile the height of the marine aerosol boundary layer (MABL) and planetary boundary layer  
254 (BL) has been estimated visually by looking at the vertical gradients of T,  $\theta$ , and RH.  
255 Meteorological parameters have been also used to calculate the vertical profiles of the gradient  
256 Richardson number (Ri):

257 
$$\text{Ri} = \frac{g}{\theta} \frac{\partial \theta}{\partial z} \bigg/ \left( \left( \frac{\partial U}{\partial z} \right)^2 + \left( \frac{\partial V}{\partial z} \right)^2 \right) \quad (2).$$

258 In Eq. (2) g is the gravitational acceleration and z is the height. The Ri number is the ratio between  
259 the buoyancy force and the wind shear and it is used to indicate dynamic stability and the formation  
260 of clear air turbulence. Turbulence can develop when Ri is below the critical threshold  $\text{Ri}_{\text{crit}}=0.25$ ,  
261 while it is inhibited for  $\text{Ri}>1$  (e.g., Wallace and Hobbs, 2006). In this study the profiles of Ri are  
262 used to provide indications of favorable/unfavorable conditions for the development of turbulent  
263 conditions within the atmosphere.

264

### 265 **3.6 Tracking the air mass back-trajectories**

266 The Lagrangian trajectory model FLEXTRA (FLEXible TRAjectories, Stohl et al., 1995) has been  
267 used in selected cases to track the origin of sampled air masses. Five days three-dimensional back-  
268 trajectories have been calculated using the ECMWF (European Centre for Medium-Range Weather  
269 Forecast) operational analysis with a  $0.5^\circ$  by  $0.5^\circ$  horizontal resolution and up to 30 vertical model  
270 levels below 4000 m. The model specific humidity and potential vorticity is also interpolated along  
271 the trajectory path.

272

### 273 **4. Meteorological conditions, aerosol load, and pollution export regimes**

274 In order to characterize the general aerosol conditions encountered over the Western Mediterranean  
275 basin during the TRAQA and the SAFMED campaigns we have plotted the time-series of the  
276 aerosol optical depth ( $\tau$ ,  $\pm 0.02$ ) at 440 nm and the 440-870 nm Ångström exponent ( $\alpha$ ) measured  
277 with a Cimel sunphotometer (Holben et al., 1998) at the three AERONET stations of Barcelona,  
278 Frioul, and Ersal located along the coast around the Western basin (see Fig. 1). Level 1.5 cloud-  
279 screened data are used in this study. Data are shown in Fig. 2 and correspond to the period of the  
280 campaign of measurements plus 10 days before and after. Table 1 reports the date, location, and  
281 main meteorological and export conditions encountered during TRAQA and SAFMED flights.

282 Over the analysed AERONET sites the aerosol optical depth was below 0.2 before the beginning of  
283 the TRAQA campaign and increased, especially at Barcelona and Ersal, to  $\sim 0.3$ - $0.5$  (with  $1 < \alpha < 2$ ) in  
284 the periods 23-26 June and 3-13 July 2012. Isolated peaks of  $\tau$  were measured in correspondence of  
285 two Saharan dust intrusion events which occurred on the 17-23 June ( $\tau \sim 0.6$ ) and 29 June 2012  
286 ( $\tau \sim 1.4$ ). Different wind regimes occurred during TRAQA and favoured the continental outflow  
287 from different regions located around the basin. Two examples of wind maps derived from WRF-  
288 Chem model (Grell et al., 2005) at 925 mbar are shown in Fig. 3 for 26 June and 3 July 2012. Main  
289 observed meteorological/export conditions can be summarized as follows: (i) on 26-27 June

290 north/north-westerly winds blew across northern Italy determining an air mass outflow towards the  
291 Gulf of Genoa (measurements on flights V18-V19-V21); (ii) on the same days a strong Mistral-  
292 Tramontane episode (i.e., strong northerly winds developing along the Rhône and Aude valley  
293 which bring a northerly/north-westerly flow over the Western Mediterranean, see Fig 3a) favoured  
294 the dispersion of pollutants towards the central part of the Western basin. Measurements during the  
295 event were performed during flight V20; (iii) on 3-4 July the wind regime was dominated by  
296 westerly/south-westerly winds mostly blowing at the surface across the Iberian Peninsula and  
297 southwestern France (see Fig. 3b). This condition allowed measuring the export of pollution from  
298 the Spanish coasts, in particular close to the area of Barcelona (flights V24-V25-V26, see Fig. 1).  
299 Additionally, flight V31 sounded the atmospheric structure close to the Spanish coasts reaching the  
300 southern urban area of Valencia. The flight was performed under the influence of south-westerly  
301 winds favouring the export from the Iberian Peninsula towards the basin; (iv) Mistral episodes  
302 occurred on the 6-7 and 11 July 2012. In those cases the Mistral wind combined with a persistent  
303 westerly flow thus yielding pollution export towards the central and central-eastern part of the  
304 Western basin, as measured during flights V27-V28-V30-V32; (v) finally, Saharan dust aerosols  
305 were sampled during flights V16 and V20 (episode of the 17-23 June) and flights V22 and V23  
306 (episode of the 29 June).

307 During SAFMED the meteorological conditions were more stable and two distinct phases were  
308 observed: (i) a stable anticyclone affected the whole Western Mediterranean area during the first  
309 half of July until the 26th, thus possibly favouring a more pronounced accumulation of  
310 photochemical pollution in this part of the basin. Relatively high values of both  $\tau$  (~0.2-0.8) and  $\alpha$   
311 (~1-2.5) were measured at the three sites of Barcelona, Frioul, and Ersa in this period; (ii) a  
312 cyclonic system moving from the Atlantic region towards Europe then affected the Western basin  
313 on 28-29 July 2013. Very clean conditions ( $\tau < 0.1-0.2$ ) were measured afterwards over the entire  
314 region until the end of the SAFMED campaign. Winds were mostly westerly/south-westerly in the

315 first period of the campaign (24-29 July 2013, flights V46, V47, V48, V49, V50), which means that  
316 the sampled air flow came mostly from the sea. Then, from 30 July to 1 August 2013 a north-  
317 easterly flow affected the SAFMED investigated area thus promoting the export of pollution from  
318 Northern Italy towards the Gulf of Genoa (flights V51, V52). A strong Mistral event (29 July-1  
319 August) and two Saharan dust outbreaks (27-28 July and 1 August) affected the Western basin,  
320 however not influencing the vertical profile observations during SAFMED.

321 In order to identify the distribution of observations during TRAQA and SAFMED as a function of  
322 the aerosol type we have plotted in Figure 4 the distribution of the measured scattering coefficient  
323  $\sigma_s$  at 450, 550, and 700 nm as a function of the calculated scattering Ångström exponent  $\alpha_s$  for all  
324 vertical profiles. The plot shows a similar scattering intensity between cases dominated by coarse  
325 particles ( $\alpha_s < 0.5-1.0$ ), such as desert dust, and those dominated by fine particles ( $\alpha_s > 1.0-1.5$ ), such  
326 as pollution aerosols. For both dust and pollution  $\sigma_s$  peaks at about  $100-120 \text{ Mm}^{-1}$ . The frequency of  
327 occurrence of  $\alpha_s$  shows that pollution plumes represent the large majority of the cases observed,  
328 with more than 70% of measurements with  $\alpha_s > 1.0$ .

329

## 330 5. Results

331 Figure 5 shows the box and whisker plots of the aerosol scattering coefficient  $\sigma_s$  at 450, 550, and  
332 700 nm, particle number concentration in the Aitken ( $dN_{\text{Aitken}}$ ) and accumulation ( $dN_{\text{Acc}}$ ) diameter  
333 ranges, and CO and O<sub>3</sub> measured in the boundary layer (BL) and in the free troposphere (FT) within  
334 pollution plumes for all the different vertical soundings analysed in this study. This plot summarizes  
335 the range of values observed during TRAQA and SAFMED. On average, the scattering coefficient  
336 and CO are larger in the BL compared to the FT, whilst similar ranges of values are measured in the  
337 two regions for  $dN_{\text{Aitken}}$ ,  $dN_{\text{Acc}}$ , and O<sub>3</sub>. Even within the single BL and FT the different parameters  
338 show a large variability that will be explored in the following paragraphs.

339

## 340 **5.1 Vertical profiles of aerosol concentration and scattering coefficient**

341 Figure 6 shows the vertical profiles of  $\sigma_s$ ,  $dN_{Acc}$ , and  $dN_{Coarse}$  during TRAQA and SAFMED flights.  
342 The date, time and coordinates of each profile, as well as the heights of the top of the marine and  
343 planetary boundary layer (MABL and BL) estimated from meteorological data are also indicated in  
344 the plot.

345 For the different vertical soundings the particle concentrations  $dN_{Acc}$  and  $dN_{Coarse}$  vary in the range  
346  $\sim 30$ - $3200 \text{ scm}^{-3}$  and  $\sim 5$ - $4000 \text{ scm}^{-3}$ , respectively, for plumes with  $\sigma_s$  between  $10$  and  $120 \text{ Mm}^{-1}$ .  
347 The structure in the scattering profile is generally mirrored in  $dN_{Acc}$  profile, and this also reflects the  
348 pronounced spectral variability (i.e., decrease for increasing wavelength) of the scattering  
349 coefficient, typical of pollution/anthropogenic particles.  $dN_{Coarse}$  also contributes to the scattering  
350 signal in some cases especially at high altitudes (see V16, V20, V21, V22, and V23 above  $\sim 2000$   
351 m), and this reflects the low spectral variability of the scattering coefficient. These observations are  
352 associated to the dust intrusion episodes which occurred in the Western Mediterranean basin during  
353 TRAQA, which however will not be analysed in detail here. Aerosol layers affected by dust have  
354 been labelled with a “D” in Fig. 6.

355 Maxima of the scattering coefficient have been measured for TRAQA flights V21 and V23 ( $\sim 120$   
356  $\text{Mm}^{-1}$  for pollution in the BL and  $\sim 100 \text{ Mm}^{-1}$  in the dust layer), whereas flights V46-V48-V49,  
357 during the first and more polluted phase of SAFMED, are the richest in  $dN_{Acc}$  ( $1500$ - $3000 \text{ scm}^{-3}$   
358 over the whole column). Minima of  $\sigma_s$  and  $dN_{Acc}$  are obtained for flight V51 at the beginning of the  
359 second SAFMED phase when clean conditions were observed in the Western Mediterranean.

360 Pollution plumes observed in the different flights extend from the boundary layer to the free  
361 troposphere up to  $3000$ - $4000$  m altitude. The vertical structure of the aerosol scattering  
362 coefficient/particle concentration is linked to the variability of the atmospheric thermodynamic  
363 structure and is generally characterized by a first layer confined in the MABL ( $<400$  m, profiles  
364 V16, V20, V22, V25, V48, V51), followed by one or more layers within the BL. In the FT pollution

365 particles occur both as single isolated plumes each about 500-1000 m deep (V21, V24, V25, V30,  
366 V46, V49), or as a more uniform layer extending from the top of the BL up to 2500-4000 m altitude  
367 (V26, V27, V28, V32, V48). The highest values of both the scattering coefficient and  $dN_{Acc}$  for  
368 pollution are found within the MABL or BL in most cases, while a local minimum of  $\sigma_s$  and  $dN_{Acc}$   
369 is generally identified at the top of the BL. The scattering coefficient and the particle concentration  
370 measured in the FT are comparable with the values observed in the BL, and in few cases even larger  
371 (V25, V26, V30). Only in one case (profile V31)  $\sigma_s$  and  $dN_{Acc}$  decrease monotonically with height.  
372 The aerosol vertical distribution, both in the BL and in the FT, often presents a strongly stratified  
373 structure characterized by the presence of several thin sub-layers within one main identified aerosol  
374 plume, as it can be seen in particular in the  $dN_{Acc}$  profiles (V20, V21, V22, V25, V46, V49).

375 The particle concentration in the Aitken mode (0.004-0.1  $\mu\text{m}$ ;  $dN_{Aitken}$ , not shown in Fig. 6) is  
376 generally below 5000-6000  $\text{scm}^{-3}$  at all altitudes up to 4000 m within pollution plumes.  $dN_{Aitken}$  is  
377 correlated with  $dN_{Acc}$  in most of the observed cases, which indicates the common source of particles  
378 in these two size ranges. Few layers exceeding  $\sim 10000\text{-}15000 \text{ scm}^{-3}$  are observed occasionally both  
379 in the BL and in the FT. These will be discussed in more detail in Sect. 5.4.

380 The  $dN_{Acc}$  and  $dN_{Aitken}$  measurements within the BL and in the FT over the sea are comparable with  
381 the values measured close to the surface at continental sites under pollution conditions (see Table 2)  
382 (Petzold et al., 2002; Mallet et al., 2003 and 2005; Wiegner et al., 2006; Junkermann, 2009;  
383 Hamburger et al., 2012; Highwood et al., 2012). This suggests that the export towards the basin  
384 favours the redistribution of the pollution plumes along the vertical. Because of mixing in the BL,  
385 measured concentrations within the BL can be as high as those observed close to the surface over  
386 the continents. Values of  $dN$  as high as in the BL are observed in the FT because of transport in  
387 specific conditions, as discussed below.

388 The observations of aerosol profiles obtained during TRAQA and SAFMED are representative of  
389 the complex transport regimes which characterizes the export towards the Western basin and that is



390 mostly determined by the interaction between regional meteorology and local dynamics (e.g.,  
391 Gangoiti et al., 2001). A first example is associated to the measurements in the area of Barcelona.  
392 As discussed in Pérez et al. (2004) the presence of mountains up to ~500-3000 m altitude a few  
393 kilometres inland favours, during summertime, the recirculation of pollutants along the coasts of  
394 Spain. In these cases, the aerosols emitted at the surface in coastal areas are transported inland and  
395 uplifted by sea breezes and mountain winds then the plumes are re-injected at different altitudes and  
396 distances from the coast. During the TRAQA flights V24, V25, and V26, under the influence of  
397 pollution outflow from the Barcelona area, we detected the presence of aerosol layers with elevated  
398 concentrations ( $dN_{Acc} \sim 2000-3000 \text{ scm}^{-3}$ ) up to 3500 m altitude at a distance of ~30 to 250 km from  
399 the coast of Spain. Another example of complex dynamics linked to coastal orography is that  
400 associated to the export from northern Italy and the Po Valley towards the Gulf of Genoa. The  
401 presence of the Apennine Mountains close to the Ligurian coasts (max elevation ~1500-2000 m)  
402 causes the uplift of continental air masses so determining the injection of aerosol plumes at different  
403 altitudes both inside and outside the BL. Examples are given by flights V19, V21 and V52 for  
404 which pollution aerosols from northern Italy are measured up to ~2000-3000 m altitude throughout  
405 the Gulf of Genoa. Finally, another meteorological condition which largely influences the aerosol  
406 export and distribution over the Western Mediterranean is the Mistral/Tramontane wind regime.  
407 Under the influence of the Mistral flow, atmospheric aerosols can be dispersed as far as hundreds of  
408 kilometres over the open sea, as discussed by Salameh et al. (2007). Examples are given in profiles  
409 V20 and V28, performed at more than 100 km from the French coasts, for which pollution layers  
410 associated to a Mistral flow are measured up to 2000-3000 m altitude.

411

## 412 **5.2 Trace gases vertical profiles**

413 Figure 7 shows O<sub>3</sub> versus CO for all TRAQA and SAFMED flights, while examples of CO and O<sub>3</sub>  
414 profiles representatives of different conditions are reported in Fig. 8 and 10.

415 CO and O<sub>3</sub> vary in the range 60-165 ppbv and 30-85 ppbv, respectively. The 25<sup>th</sup> and 75<sup>th</sup>  
416 percentiles are 87 and 105 ppbv for CO and 49 and 62 ppbv for O<sub>3</sub>, representative of moderate  
417 pollution conditions (i.e., Parrish et al., 1998). By comparison, the values measured over land in  
418 central Italy during flight V49 are in the range 80-180 ppbv for carbone monoxide and 40-85 ppbv  
419 for ozone. CO and O<sub>3</sub> are generally correlated (correlation coefficient R<sup>2</sup>~0.5-0.8) within measured  
420 pollution plumes, and also correlated with  $\sigma_s$  and N<sub>Acc</sub> both in the BL and in the FT, which indicates  
421 photochemically active plumes. CO is generally higher in the BL, and shows absolute maxima in  
422 the lowest levels (V20, V21, V24, V28, V46), then it decreases in the FT. Ozone presents a more  
423 complicated vertical structure due to the different photochemical and dynamical processes which  
424 control its formation and distribution. At first, local peaks of O<sub>3</sub> correlated with CO are observed in  
425 correspondence of pollution plumes both in the BL and in the FT. An absolute maximum of O<sub>3</sub> is  
426 sometimes found near the top of the BL (V24, V25, V30) possibly due to aged air masses trapped in  
427 the boundary layer. Isolated peaks of O<sub>3</sub> (~75-80 ppbv) not correlated with aerosols and CO are also  
428 measured in few cases above 3000-3500 m (V21, V25, V27, V28, V52). The analysis of back-  
429 trajectories indicates that these high-altitude ozone layers are associated to the descent of air masses  
430 travelling at about 7-8 km, which thus may suggest a downward transport from the upper  
431 troposphere or the tropopause region due to a stratosphere-troposphere exchange (Ancellet and  
432 Ravetta, 2005). Finally, absolute minima of O<sub>3</sub> (~15-30 ppbv) are measured within the dust layers  
433 during flights V20 and V21, maybe related to the dust/ozone heterogeneous reactions which leads  
434 to O<sub>3</sub> destruction, as documented in several studies (Bonasoni et al., 2004; Haywood et al., 2011).

435

### 436 **5.3 $\Delta O_3/\Delta CO$ and $dN_{Aitken}/dN_{Acc}$ ratios and variability of pollution plume composition**

437 Using the O<sub>3</sub>, CO,  $dN_{Aitken}$  and  $dN_{Acc}$  measurements we have estimated:

- 438 - the O<sub>3</sub>-CO enhancement ratio ( $\Delta O_3/\Delta CO$ ), i.e. the ratio of the ozone to carbon monoxide  
439 variations compared to their baseline values. The  $\Delta O_3/\Delta CO$  enhancement ratio is frequently

440 used to estimate the efficiency of O<sub>3</sub> formation and its export (Parrish et al., 1993; Zhang et  
441 al., 2006). From our observations (Fig. 7) we have estimated a background value of ~70  
442 ppbv in the BL and 60 ppbv in the FT for CO and ~30 ppbv for O<sub>3</sub> both in the BL and in the  
443 FT.

444 - The Aitken to accumulation number ratio ( $dN_{\text{Aitken}}/dN_{\text{Acc}}$ ), which defines the relative  
445 importance of particles in the Aitken and accumulation modes.  $dN_{\text{Aitken}}$  is generally  
446 associated to gas-to-particle conversion and nucleation events and is higher in fresh plumes,  
447 while it decreases with the increasing of the plume lifetime due to coagulation or  
448 condensation of water-soluble chemical species on the particle surface (Kulmala et al.,  
449 2004).

450 The combination of  $\Delta O_3/\Delta CO$  and  $dN_{\text{Aitken}}/dN_{\text{Acc}}$  has been used to retrieve additional information  
451 on the atmospheric vertical structure, layering, and particle aging.

452 Within detected pollution plumes the  $\Delta CO$  and  $\Delta O_3$  reach up to 100-120 ppbv and 45-55 ppbv,  
453 respectively, with a corresponding  $\Delta O_3/\Delta CO$  ratio which varies in the range ~0.10-2.0 for all cases.  
454 These values are comparable with the range of observations available in the literature for fresh and  
455 moderately aged pollution plumes in the BL and in the lower FT (~0.2-1.0) (Chin et al., 1994;  
456 Parrish et al., 1998; Zhang et al., 2006; Cristofanelli et al., 2013).  $dN_{\text{Aitken}}/dN_{\text{Acc}}$  is between about 1  
457 and 20 in most of pollution cases, which indicates the presence of both fresh layers rich in Aitken  
458 particles and aged plumes poor in Aitken particles. Extremely high values of  $dN_{\text{Aitken}}/dN_{\text{Acc}}$  (~50-  
459 200) are measured in few cases in layers with very low  $dN_{\text{Acc}}$  concentrations.

460 The large variability in  $\Delta O_3/\Delta CO$  and  $dN_{\text{Aitken}}/dN_{\text{Acc}}$  indicates a strong heterogeneity in terms of  
461 composition and lifetime for the different observed plumes. This heterogeneity reflects the  
462 complexity in terms of sources, production processes, and transport mechanisms which  
463 characterizes the Western basin. In order to illustrate this point, we have selected three examples  
464 representative of different conditions observed in different areas of the basin: (i) V19, performed in

465 the Gulf of Genoa in correspondence of continental outflow events from Northern Italy/Po Valley;  
466 (ii) V20, performed in Southern France during a Mistral event; (iii) V24, which measured the export  
467 of pollution from the area of Barcelona. The vertical profiles of the spectral scattering coefficient  $\sigma_s$ ,  
468 temperature T, relative humidity RH,  $dN_{Acc}$ ,  $dN_{Aitken}$ , CO, O<sub>3</sub>,  $\Delta O_3/\Delta CO$ ,  $dN_{Aitken}/dN_{Acc}$  and wind  
469 are reported in Fig. 8 for these cases.

470 *1. V19: export from northern Italy/Po Valley.* The profile shown for flight V19 (Fig. 8a) is  
471 characterized by the presence of three different aerosol structures: the first one below 800 m,  
472 characterized by a lower  $dN_{Aitken}/dN_{Acc}$  (~1-5) and relatively high  $\Delta O_3/\Delta CO$  (~0.4-1.5), possibly  
473 associated to moderately aged pollution; the second one between 800 and 2600 m, richer in fine  
474 particles ( $dN_{Aitken}/dN_{Acc}$ ~5-15), so possibly linked to fresher emissions; and the third one above  
475 2600 m, where the ratio  $dN_{Aitken}/dN_{Acc}$  rises rapidly, as will be further discussed in Sect. 5.4. The  
476 export of fresh pollution at 800-2600 m from northern Italy as observed in V19 may be related to  
477 the peculiar orography of this region and the uplift of continental air masses. This is confirmed by  
478 the analysis of the back-trajectories (Fig. 9) which indicates that the air masses arriving at 1000 and  
479 2000 m passed over the western Po Valley at an altitude of about 400-1200 m and were then  
480 uplifted near the Ligurian coast to enter the basin above the BL. Junkermann (2009) measured high  
481 levels of fine particles up to about 2000 m in the western Po Valley, which means that the altitudes  
482 of 400-1200 m reached by our investigated air masses could have been sufficient for them to collect  
483 fresh emitted particles along their path. Conversely, below 800 m the air mass trajectory shows a  
484 longer subsidence over the sea surface in the troposphere which has possibly favoured the advection  
485 of more aged plumes, or the mixing with sea salts thus inducing the decrease of the  $dN_{Aitken}/dN_{Acc}$   
486 ratio. It should be noted that the aerosol layer in the FT also shows relatively higher values of the  
487  $\Delta O_3/\Delta CO$  ratio (~0.6-1.0) compared to the more aged plume in the BL. The enhanced amount of O<sub>3</sub>  
488 in this air mass can be linked to a high concentration of volatile precursors which may have  
489 favoured the build-up of ozone during the plume evolution. In a recent work, Kaiser et al. (2014)

490 suggest that in the Po Valley the high content of formaldehyde, also observed by Junkermann et al.  
491 (2009), may be responsible for the excess of O<sub>3</sub> production. Fresh layers in the FT up to ~2000-  
492 3000 m possibly associated to pollution export from northern Italy have been also observed during  
493 flights V21 and V52 (not shown).

494       2. *V20: export during a Mistral/Tramontane event.* V20 provides an example of export during a  
495 Mistral/Tramontane event. As shown in Fig. 8b, winds from the northwest direction are measured at  
496 all altitudes during flight V20. The aerosol profile in the BL is characterized in the first ~400 m by  
497 the presence of a layer richer in dN<sub>Aitken</sub> (dN<sub>Aitken</sub>/dN<sub>Acc</sub>>20) and CO (100 ppbv close to the surface;  
498 CO data not available between 150 and 650 m) possibly linked to fresh pollution, followed by the  
499 alternation of several layers characterized by a variable dN<sub>Aitken</sub> (1000-6000 scm<sup>-3</sup>) and lower CO  
500 (~70 ppbv). A local minimum of dN<sub>Aitken</sub> and σ<sub>s</sub> is found at ~400 m. For all these layers the O<sub>3</sub> is  
501 very low (~30-40 ppbv) and the ΔO<sub>3</sub>/ΔCO ratio is <0.6-0.8. At higher altitudes, between 1400 and  
502 2000 m, we observe a layer enriched in O<sub>3</sub> (ΔO<sub>3</sub>/ΔCO~1-2) in correspondence of an almost aerosol-  
503 free region. This enriched ozone layer might be possibly associated to a downward transport from  
504 higher tropospheric layers, as also suggested by the back-trajectories (Fig. 9), as well as to the  
505 mixing with ozone rich layers along the air mass trajectory. Larger particles, from long-range  
506 transport of Saharan dust at latitudes below 30° N, are measured between 2000 and 3000 m, with a  
507 minimum of O<sub>3</sub> (~15-20 ppbv) registered within the layer. Several other flights were performed  
508 during Mistral/Tramontane episodes (V27, V28, V30, V32) and show, similarly to V20, the  
509 presence of several layers both in the BL and the FT.

510       3. *V24: export from the Barcelona area.* Measurements during V24 may be taken as representative  
511 of local recirculation (Pérez et al., 2004). In the V24 profile in Fig. 8c we may recognize up to 5  
512 different aerosol layers. A first layer at <200 m within the MABL, coming from the southwest and  
513 directly exported from the area of Barcelona. The layer is characterized by high CO (90-120 ppbv),  
514 and relatively low values of dN<sub>Aitken</sub> (~4000 scm<sup>-3</sup>) and O<sub>3</sub> (~50 ppbv), which possibly suggest the

515 mixing of pollution with marine particles close to the sea surface. A second layer of fresher  
516 particles, always coming from the southwestern direction, is observed above the MABL between  
517 200 and 600 m ( $dN_{\text{Aitken}} \sim 6000\text{-}8000 \text{ scm}^{-3}$ ,  $O_3 \sim 70 \text{ ppb}$ , with  $dN_{\text{Aitken}}/dN_{\text{Acc}} \sim 5\text{-}15$ , and  
518  $\Delta O_3/\Delta CO \sim 0.8\text{-}1.5$ ). A third, more aged, sublayer ( $dN_{\text{Aitken}}/dN_{\text{Acc}} \sim 2\text{-}5$ ,  $\Delta O_3/\Delta CO \sim 0.8\text{-}1.0$ ) is  
519 observed within the BL between 600 and 1000 m. The FT is characterized by the presence of  
520 moderately aged plumes from  $\sim 1000$  to 2800 m ( $dN_{\text{Aitken}}/dN_{\text{Acc}} \sim 2\text{-}10$ ,  $\Delta O_3/\Delta CO \sim 0.2\text{-}0.8$ ), and a  
521 very aged plume at 2800-3800 m almost deprived in Aitken particles and richer in  $O_3$   
522 ( $dN_{\text{Aitken}}/dN_{\text{Acc}} < 1$ ,  $\Delta O_3/\Delta CO \sim 0.6\text{-}1.5$ ). A marked local minimum is observed at the top of the BL  
523 for  $\sigma_s$ ,  $dN_{\text{Acc}}$ ,  $dN_{\text{Aitken}}$ , CO, and  $O_3$ , suggesting the presence of air masses with different origin  
524 between the BL and the FT. This is also confirmed by the analysis of the back-trajectories (Fig. 9)  
525 which indicates a low level air masses coming from the Spanish coasts in the BL, and air masses  
526 travelling at higher altitudes in the FT. In particular, the layer at 2800-3800 m is possibly associated  
527 to an intercontinental transport from Northern America, as shown in the trajectory ending at 3500  
528 m. A similar structure characterized by the alternation of fresher and more aged plumes in the BL  
529 and FT is also observed in V25 for which aerosol layers are detected up to 4000 m altitude.

530 The detailed analysis of these three events evidences the complexity of the atmospheric structure  
531 over the Western Mediterranean basin in link with the different dynamical processes involved.

532

#### 533 **5.4 Layers with enhanced Aitken mode particle numbers**

534 Isolated layers with  $dN_{\text{Aitken}} \sim 10000\text{-}15000 \text{ scm}^{-3}$  have been observed occasionally both in the BL  
535 and in the FT. The vertical profiles of  $dN_{\text{Aitken}}$  for some selected cases are shown in Fig. 10.

536 For about half of the observed events the  $dN_{\text{Aitken}}$  layer appears related to a simultaneous increase in  
537  $dN_{\text{Acc}}$ , CO, and  $O_3$ , which suggests that the layer has been transported from a region directly  
538 emitting in this size range. These cases are: V16 at  $\sim 200\text{-}400$  m, V21 at  $\sim 400\text{-}800$  m, V28 at  $\sim 250$   
539 m, and V31 at  $\sim 1000\text{-}3000$  m (only V28 and V31 are shown in Fig. 10). The most remarkable

540 example is V31 (Fig. 10a), performed close to the coasts of Spain near Valencia, for which the high  
541  $dN_{\text{Aitken}}$  layer extends from the top of the BL to ~3000 m altitude. The wind vector and the back-  
542 trajectories (not shown) indicates that the air mass comes from the western-southwestern direction  
543 above 1000 m, so the  $dN_{\text{Aitken}}$  layer can be directly related to pollution export from the urban region  
544 of Valencia.

545 In all the other cases the high  $dN_{\text{Aitken}}$  layer is generally not related to simultaneous  $dN_{\text{Acc}}$  and  $\text{O}_3$   
546 increase. Two of these cases (V16 at ~800-1000 m and V28 at ~100 m) occur in the BL.

547 For the V28 layer (Fig. 10b) the  $dN_{\text{Aitken}}$  is correlated with CO which might indicate the influence of  
548 local emissions close to the surface level (i.e., ship emissions). CO values are relatively high (140-  
549 160 ppbv) within the layer. It has been often assumed that new particle formation events (NPF) only  
550 occur in almost clean environments (e.g., O'Dowd et al., 2010; Sellegri et al., 2010), and that they  
551 are suppressed under polluted conditions. In a recent study, Brines et al. (2014) show the occurrence  
552 of NPF events also in urban areas with high level of pollution in the Mediterranean region. So, we  
553 explore the possibility of NPF in our observations. Given the size ranges of the CPC and PCASP,  
554 however, we cannot discriminate within  $dN_{\text{Aitken}}$  the particle concentration in the sole 4-20 nm  
555 range, i.e. the size range involved in nucleation. So it is not possible to directly associate the V28  
556 observations to NPF. In order to obtain a qualitative indication of the possible occurrence of NPF,  
557 we have looked at the air mass dynamics within the layer. Several studies suggest, in fact, that NPF  
558 might be favoured by turbulence and air mass mixing (e.g., Nilsson et al., 2001; Wehner et al.,  
559 2010). We have thus looked at the gradient Richardson number (Ri) which gives information on the  
560 atmospheric dynamical stability. Vertical profiles of Ri are also shown in Fig. 10. For V28 the  
561 vertical profile of Ri indicates that below 200 m the Ri number is consistently below zero, which  
562 suggests well established turbulent conditions possibly favouring NPF in this layer.

563 In other two cases (V19, Fig. 10c, and V26, Fig. 10d), under lower pollution conditions ( $\text{CO} < 100$ ),  
564 we measured high  $dN_{\text{Aitken}}$  concentration in correspondence of low  $dN_{\text{Acc}}$  layers in the FT at ~2800-

565 3000 m for V19 and 3500-4500 m for V26. For V19 and V26 layers,  $dN_{\text{Aitken}}$  seems anticorrelated  
566 to CO. Also in this case the Richardson number is below  $Ri_{\text{crit}}$  in correspondence of the Aitken peak  
567 meaning that conditions are favorable for turbulence within the layer, and this may indicate also in  
568 this case the possible role of NPF.

569 Finally, a case of high  $dN_{\text{Aitken}}$  concentration has been also observed in correspondence of dust  
570 particles between ~3000 and 4000 m (V23b, Fig. 10e). This layer can be possibly linked to the  
571 photochemically-induced nucleation which may occur in presence of dust and  $\text{SO}_2$  as hypothesised  
572 in a recent study by Dupart et al. (2012) and observed by Nie et al. (2014).

573

## 574 **6. Conclusions**

575 The data presented in this paper gives an overview of the distribution of aerosols and trace gases  
576 within the tropospheric column up to 5000 m above the Western Mediterranean basin.

577 These data add to the very few available measurements of aerosol and trace gases vertical profiles  
578 over the sea surface in the Central (e.g., Junkermann, 2001; Meloni et al., 2003; Di Iorio et al.,  
579 2003; Pace et al., 2014) and Eastern (e.g., Formenti et al., 2002; Dulac and Chazette, 2003) parts of  
580 the basin thus contributing to improve the description of the atmospheric composition and structure  
581 over the whole Mediterranean area.

582 Observations from the present study indicate that continental pollution strongly affects the  
583 composition and structure of the Western Mediterranean basin both close to coastal regions and in  
584 the open sea. Pollution layers extend up to 250 km far from the coasts and reach up to 3000-4000 m  
585 altitude, presenting a complex and highly stratified structure. The measured particle concentration is  
586 comparable with the values reported for continental Europe (Petzold et al., 2002; Junkermann,  
587 2009; Hamburger et al., 2012).



588 Pollution plumes with different compositions, origins, and lifetimes are observed in link with the  
589 different observed dynamical export conditions and meteorological regimes. The aerosol and trace  
590 gas observations during TRAQA and SAFMED are consistent with the results of former campaigns  
591 and with the interpretation of observed or well known air-masses dynamics and meteorological  
592 phenomena that can occur in the Western basin (Flamant and Pelon, 1996; Millan et al., 1997;  
593 Gangoiti et al., 2001; Pérez et al., 2004; Mallet et al., 2005).

594 The large heterogeneity in aerosol compositions, origins, and lifetimes as documented in this study  
595 can reflect in a large heterogeneity of aerosol optical properties, with consequences for their direct  
596 radiative effect in this part of the basin. This aspect will be investigated in a companion paper  
597 analysing the TRAQA and SAFMED in situ measurements of the aerosol absorption and scattering  
598 properties and their variability.

599 From the present observations, it is also interesting to note the relatively high values of  $dN_{\text{Aitken}}$   
600 measured both in the BL and the FT, which evidences the important contribution of ultrafine  
601 particles at all altitudes over the basin. These can be linked to the different export mechanisms  
602 previously discussed, as well as the possible occurrence of NPF events. Aitken particle profiles are  
603 very rare over the sea surface in the Mediterranean (e.g., Junkermann et al. 2001; Pace et al., 2015)  
604 and data comparison is quite difficult. Few studies have observed NPF in the FT in continental  
605 areas (Boulon et al., 2010; Rose et al., 2014) and suggest that the export of pollution into the upper  
606 troposphere, as it is common in the Western basin, might promote the occurrence of these events.  
607 The observations of the present study may thus also have very large implications due to the crucial  
608 role of NPF in controlling the atmospheric cloud condensation nuclei concentration (Spracklen et  
609 al., 2008) and the associated aerosol indirect effect on climate.

610

611 **Author contributions**

612 J.-L.A., F.R., G.A., M.B., A.B., P.F. and K.S. designed the TRAQA and SAFMED experiments and  
613 coordinated the campaigns. C.G., N.G., and C.D.B operated the instruments on board the ATR-42  
614 during the flights. C.D.B. performed the data analysis with contributions from L.D., P.F., F.R.,  
615 A.B., G.A., J.-C.R., and M.B.. G.A. performed the FLEXTRA simulations. J.-C.R. performed the  
616 WRF-Chem simulations. C.D.B. wrote the manuscript.

617

## 618 **Acknowledgements**

619 All measurement presented here are from the Chemistry-Aerosol Mediterranean Experiment project  
620 (ChArMEx, <http://charmex.lsce.ipsl.fr>), which is the atmospheric component of the French  
621 multidisciplinary program MISTRALS (Mediterranean Integrated Studies at Regional And Local  
622 Scales). ChArMEx-France was principally funded by INSU, ADEME, ANR, CNES, CTC (Corsica  
623 region), EU/FEDER, Météo-France, and CEA. TRAQA was funded by ADEME/PRIMEQUAL and  
624 MISTRALS/ChArMEx programmes and Observatoire Midi-Pyrénées. SAFMED was funded by the  
625 ANR project SAF-MED (Secondary Aerosol Formation in the MEDiterranean, grant SIMI6 ANR-  
626 12-BS06-0013). C. Di Biagio thanks the Centre National des Etudes Spatiales (CNES) for financial  
627 support.

628 The authors wish to thank the technicians, pilots and ground crew of SAFIRE (Service des Avions  
629 Français Instruments pour la Recherche en Environnement) for facilitating the instrument  
630 integration and conducting flying operations. We thank S. Chevaillier, L. Girault, R. Loisil, J.  
631 Pelon, S. Triquet, and P. Zapf for their contribution during the campaigns. We thank S. Basart, J.  
632 M. Baldasano, M. Mallet, P. Goloub, J. Piazzola and their staff for establishing and maintaining the  
633 Barcelona, Ersa, and Frioul AERONET sites. Helpful discussions with G. Pace are gratefully  
634 acknowledged. We thank also two anonymous reviewers whose suggestions helped to clarify the  
635 manuscript.

636

638 **References**

- 639 Ancellet, G. and Ravetta, F.: Analysis and validation of ozone variability observed by lidar during  
640 the ESCOMPTE-2001 campaign, *Atmos. Res.*, 74, 435–459, 2005.
- 641 Anderson, T. L., Covert, D. S., Marshall, S. F., Laucks, M. L., Charlson, R. J., Waggoner, A. P.,  
642 Ogren, J. A., Caldow, R., Holm, R. L., Quant, F. R., Sem, G. J., Wiedensholer, A., Ahlquist, N.  
643 A., and Bates, T. S.: Performance characteristics of a high-sensitivity, three-wavelength, total  
644 scatter/backscatter nephelometer, *J. Atmos. Ocean. Tech.*, 13, 967–986, 1996.
- 645 Anderson, T. L. and Ogren, J. A.: Determining aerosol radiative properties using the TSI 3563  
646 integrating nephelometer, *Aerosol Sci. Technol.*, 29, 57–69, 1998.
- 647 Bonasoni, P., Cristofanelli, P., Calzolari, F., Bonafè, U., Evangelisti, F., Stohl, A., Zauli Sajani, S.,  
648 van Dingenen, R., Colombo, T., and Balkanski, Y.: Aerosol-ozone correlations during dust  
649 transport episodes, *Atmos. Chem. Phys.*, 4, 1201-1215, doi:10.5194/acp-4-1201-2004, 2004.
- 650 Boucher, O., Randall, D., Artaxo, P., Bretherton, C., Feingold, G., Forster, P., Kerminen, V.-M.,  
651 Kondo, Y., Liao, H., Lohmann, U., Rasch, P., Satheesh, S. K., Sherwood, S., Stevens, B., and  
652 Zhang, X. Y.: Clouds and Aerosols. In: *Climate Change 2013: The Physical Science Basis*.  
653 Contribution of Working Group I to the Fifth Assessment Report of the Intergovernmental Panel  
654 on Climate Change [Stocker, T.F., D. Qin, G.-K. Plattner, M. Tignor, S.K. Allen, J. Boschung,  
655 A. Nauels, Y. Xia, V. Bex and P.M. Midgley (eds.)]. Cambridge University Press, Cambridge,  
656 United Kingdom and New York, NY, USA, 571-657, 2013.
- 657 Boulon, J., Sellegri, K., Venzac, H., Picard, D., Weingartner, E., Wehrle, G., Collaud Coen, M.,  
658 Bütikofer, R., Flückiger, E., Baltensperger, U., and Laj, P.: New particle formation and ultrafine  
659 charged aerosol climatology at a high altitude site in the Alps (Jungfrauoch, 3580 m a.s.l.,  
660 Switzerland), *Atmos. Chem. Phys.*, 10, 9333–9349, doi: 10.5194/acp-10-9333-2010, 2010.
- 661 Brines, M., Dall'Osto, M., Beddows, D. C. S., Harrison, R. M., Gómez-Moreno, F., Núñez, L.,  
662 Artíñano, B., Costabile, F., Gobbi, G. P., Salimi, F., Morawska, L., Sioutas, C., and Querol, X.:  
663 Frequency of new particle formation events in the urban Mediterranean climate, *Atmos. Chem.*  
664 *Phys. Discuss.*, 14, 26463-26494, doi:10.5194/acpd-14-26463-2014, 2014.
- 665 Chazette, P., Randriamiarisoa, H., Sanak, J., Couvert, P., and Flamant, C.: Optical properties of  
666 urban aerosol from airborne and ground based in situ measurements performed during the  
667 ESQUIF program, *J. Geophys. Res.*, 110, D02206, doi:10.1029/2004JD004810, 2005.
- 668 Chin, M., Jacob, D. J., Munger, J. W., Parrish, D. D., and Doddridge, B. G.: Relationship of ozone  
669 and carbon monoxide over North America, *J. Geophys. Res.*, 99, 14,565–14,573, 1994.
- 670 Colette, A., Ancellet, G., Menut, L., and Arnold, S. R.: A Lagrangian analysis of the impact of  
671 transport and transformation on the ozone stratification observed in the free troposphere during  
672 the ESCOMPTE campaign, *Atmos. Chem. Phys.*, 6, 3487-3503, doi:10.5194/acp-6-3487-2006,  
673 2006.
- 674 Cristofanelli, P., Fierli, F., Marinoni, A., Calzolari, F., Duchi, R., Burkhart, J., Stohl, A., Maione,  
675 M., Arduini, J., and Bonasoni, P.: Influence of biomass burning and anthropogenic emissions on  
676 ozone, carbon monoxide and black carbon at the Mt. Cimone GAW-WMO global station (Italy,  
677 2165 m a.s.l.), *Atmos. Chem. Phys.*, 13, 15–30, 2013.

- 678 Di Iorio, T., di Sarra, A., Junkermann, W., Cacciani, M., Fiocco, G., and Fua`, D.: Tropospheric  
679 aerosols in the Mediterranean: 1. Microphysical and optical properties, *J. Geophys. Res.*,  
680 108(D10), 4316, doi:10.1029/2002JD002815, 2003.
- 681 Drobinski, P., Saïd, F., Ancellet, G., Arteta, J. Augustin, P., Bastin, S., Brut, A., Caccia, J. L.,  
682 Campistron, B., Cautenet, S., Colette, A., Coll, I., Corsmeier, U., Cros, B., Dabas, A., Delbarre,  
683 H., Dufour, A., Durand, P., Guénard, V., Hasel, M., Kalthoff, N., Kottmeier, C., Lasry, F.,  
684 Lemonsu, A., Lohou, F., Masson, V., Menut, L., Moppert, C., Peuch, V. H., Puygrenier, V.,  
685 Reitebuch, O., and Vautard, R.: Regional transport and dilution during high-pollution episodes in  
686 southern France: Summary of findings from the Field Experiment to Constraint Models of  
687 Atmospheric Pollution and Emissions Transport (ESCOMPTE), *J. Geophys. Res.*, 112, D13105,  
688 doi:10.1029/2006JD007494, 2007.
- 689 Dulac, F., and Chazette, P.: Airborne study of a multi-layer aerosol structure in the eastern  
690 Mediterranean observed with the airborne polarized lidar ALEX during a STAAARTE campaign  
691 (7 June 1997), *Atmos. Chem. Phys.*, 3, 1817-1831, doi:10.5194/acp-3-1817-2003, 2003.
- 692 Dupart, Y.; King, S. M., Nekat, B., Nowak, A., Wiedensohler, A., Herrmann, H., David, G.,  
693 Thomas, B., Miffre, A., Rairoux, P., D'Anna, B., and George, C.: Mineral dust photochemistry  
694 induces nucleation events in the presence of SO<sub>2</sub>. *PNAS*, 109, (51), 20842–20847, 2012.
- 695 Ebert, M., Weinbruch, S., Rausch, A., Gorzawski, G., Hoffmann, P., Wex, H., and Helas, G.: The  
696 complex refractive index of aerosols during LACE 98 as derived from the analysis of individual  
697 particles, *J. Geophys. Res.*, 107, D21, 8121, doi:10.1029/2000JD000195, 2002.
- 698 Ebert, M., Weinbruch, S., Hoffmann, P., and Ortner, H. M.: The chemical composition and complex  
699 refractive index of rural and urban influenced aerosols determined by individual particle  
700 analysis, *Atmos. Environ.*, 38, 6531–6545, 2004.
- 701 Flamant, C., and Pelon, J.: Atmospheric boundary-layer structure over the Mediterranean during a  
702 Tramontane event, *Quart. J. Roy. Meteorol. Soc.*, 122, 1741–1778, 1996.
- 703 Formenti, P., Reiner, T., Sprung, D., Andreae, M. O., Wendisch, M., Wex, H., Kindred, D., Dewey,  
704 K., Kent, J., Tzortziou, M., Vasaras, A., and Zerefos, C.: STAAARTE-MED 1998 summer  
705 airborne measurements over the Aegean Sea, 1, Aerosol particles and trace gases, *J. Geophys.*  
706 *Res.*, 107, D21, doi:10.1029/2001JD001337, 2002.
- 707 Formenti, P., Rajot, J. L., Desboeufs, K., Saïd, F., Grand, N., Chevaillier, S., and Schmechtig, C.:  
708 Airborne observations of mineral dust over western Africa in the summer Monsoon season:  
709 spatial and vertical variability of physico-chemical and optical properties, *Atmos. Chem. Phys.*,  
710 11, 6387-6410, doi:10.5194/acp-11-6387-2011, 2011.
- 711 Gangoiti, G., M. M. Millán, R. Salvador, E. Mantilla: Long-Range transport and recirculation of  
712 pollutants in the Western Mediterranean during the RECAPMA Project. *Atmos. Environ.*, 35,  
713 6267-6276, 2001.
- 714 Gkikas, A., Houssos, E. E., Hatzianastassiou, N., Papadimas, C. D., and Bartzokas, A.: Synoptic  
715 conditions favouring the occurrence of aerosol episodes over the broader Mediterranean basin,  
716 *Q. J. R. Meteorol. Soc.*, 138: 932–949. doi:10.1002/qj.978, 2012.
- 717 Grell, G. A., Peckham, S. E., Schmitz, R., McKeen, S. A., Frost, G., Skamarock, W. C., and Eder,  
718 B.: Fully coupled “online” chemistry within the WRF model, *Atmos. Environ.*, 39, 6957–6975,  
719 2005.
- 720 Hamburger, T., McMeeking, G., Minikin, A., Petzold, A., Coe, H., and Krejci, R.: Airborne  
721 observations of aerosol microphysical properties and particle ageing processes in the troposphere  
722 above Europe, *Atmos. Chem. Phys.*, 12, 11533-11554, doi:10.5194/acp-12-11533-2012, 2012.

- 723 Haywood, J., Johnson, B., Osborne, S., Mulcahy, J., Brooks, M., Harrison, M., Milton, S., and  
724 Brindley, H.: Observations and modelling of the solar and terrestrial radiative effects of Saharan  
725 dust: a radiative closure case-study over oceans during the GERBILS campaign, *Q. J. R.*  
726 *Meteorol. Soc.*, 137, 1211–1226, doi:10.1002/qj.770, 2011.
- 727 Highwood, E. J., Northway, M. J., McMeeking, G. R., Morgan, W. T., Liu, D., Osborne, S.,  
728 Bower, K., Coe, H., Ryder, C., and Williams, P.: Aerosol scattering and absorption during the  
729 EUCAARI-LONGREX flights of the Facility for Airborne Atmospheric Measurements (FAAM)  
730 BAe-146: can measurements and models agree?, *Atmos. Chem. Phys.*, 12, 7251-7267,  
731 doi:10.5194/acp-12-7251-2012, 2012.
- 732 Holben, B. N., Eck, T. F., Slutsker, I., Tanré, D., Buis, J. P., Setzer, A., Vermote, E., Reagan, J. A.,  
733 Kaufman, Y., Nakajima, T., Lavenu, F., Jankowiak, I., and Smirnov, A.: AERONET: a federated  
734 instrument network and data archive for aerosol characterization, *Rem. Sens. Environ.*, 66, 1–16,  
735 1998.
- 736 Jiménez, P., Pérez, C., Rodríguez, A., and Baldasano, J. M. : Correlated levels of particulate matter  
737 and ozone in the western Mediterranean basin: Air quality and lidar measurements, 22<sup>nd</sup> Annual  
738 Conference Am. Assoc. for Aerosol Res., Anaheim, California, 20-24 October 20-24 2003,  
739 2003.
- 740 Jiménez, P., Lelieveld, J., and Baldasano, J. M.: Multiscale modeling of air pollutants dynamics in  
741 the northwestern Mediterranean basin during a typical summertime episode, *J. Geophys. Res.*,  
742 111, D18306, doi:10.1029/2005JD006516, 2006.
- 743 Jiménez-Guerrero, P., Jorba, O., Baldasano, J. M., and Gassó, S.: The use of a modelling system as  
744 a tool for air quality management: Annual high-resolution simulations and evaluation, *Sci. Tot.*  
745 *Environ.*, 390, 323–340, 2008.
- 746 Junkermann, W.: An ultralight aircraft as platform for research in the lower troposphere: System  
747 performance and first results from radiation transfer studies in stratiform aerosol layers and  
748 broken cloud conditions, *J. Atmos. Oceanic Technol.*, 18, 934–946, 2001.
- 749 Junkermann, W.: On the distribution of formaldehyde in the western Po-Valley, Italy, during 800  
750 FORMAT 2002/2003, *Atmos. Chem. Phys.*, 9, 9187-9196, doi:10.5194/acp-9-9187-2009, 2009.
- 751 Kaiser, J., Wolfe, G. M., Bohn, B., Broch, S., Fuchs, H., Ganzeveld, L. N., Gomm, S., Häsel, R.,  
752 Hofzumahaus, A., Holland, F., Jäger, J., Li, X., Lohse, I., Lu, K., Rohrer, F., Wegener, R.,  
753 Mentel, T. F., Kiendler-Scharr, A., Wahner, A., and Keutsch, F. N.: Evidence for an unidentified  
754 ground-level source of formaldehyde in the Po Valley with potential implications for ozone  
755 production, *Atmos. Chem. Phys. Discuss.*, 14, 25139-25165, doi:10.5194/acpd-14-25139-2014,  
756 2014.
- 757 Kallos, G., Astitha, M., Katsafados, P., and Spyrou, C.: Long-range transport of anthropogenically  
758 and naturally produced particulate matter in the Mediterranean and North Atlantic: Current state  
759 of knowledge, *J. Appl. Meteorol. Climatol.*, 46, 1230–1251, 2007.
- 760 Kulmala, M., Vehkamäki, H., Petaja, T., Dal Maso, M., Lauri, A., Kerminen, V.-M., Birmili, W.,  
761 and McMurry, P.H.: Formation and growth rates of ultrafine atmospheric particles: A review of  
762 observations, *J. Aerosol Sci.*, 35(2), 143–176, 2004.
- 763 Lelieveld, J., Berresheim, H., Borrmann, S., Crutzen, P. J., Dentener, F. J., Fischer, H., Feichter, J.,  
764 Flatau, P. J., Heland, J., Holzinger, R., Korrman, R., Lawrence, M. G., Levin, Z., Markowicz,  
765 K. M., Mihalopoulos, N.; Minikin, A., Ramanathan, V., de Reus, M., Roelofs, G. J., Scheeren,  
766 H. A., Sciare, J., Schlager, H., Schultz, M., Siegmund, P., Steil, B., Stephanou, E. G., Stier, P.,  
767 Traub, M., Warneke, C., Williams, J., and Ziereis H.: Global air pollution crossroads over the  
768 Mediterranean, *Science*, 298, 794–799, doi:10.1126/science.1075457, 2002.

- 769 Liu, Y. and Daum, P.: The effect of refractive index on size distributions and light scattering  
770 coefficients derived from optical particle counters, *J. Aerosol Sci.*, 31, 945–957, 2000.
- 771 Mallet, M., Roger, J. C., Despiiau, S., Dubovik, O., and Putaud, J. P.: Microphysical and optical  
772 properties of aerosol particles in urban zone during ESCOMPTE, *Atmos. Res.*, 69, 73–97, 15  
773 2003.
- 774 Mallet, M., Van Dingenen, R., Roger, J. C., Despiiau, S., and Cachier, H.: In situ airborne  
775 measurements of aerosol optical properties during photochemical pollution events, *J. Geophys.*  
776 *Res.*, 110, D03205, doi:10.1029/2004JD005139, 2005.
- 777 Mallet, M., Gomes, L., Solmon, F., Sellegri, K., Pont, V., Roger, J. C., Missamou, T., and Piazzola,  
778 J.: Calculation of key optical properties of the main anthropogenic aerosols over the Western  
779 French coastal Mediterranean Sea, *Atmos. Res.*, 101, 396–411, 2011.
- 780 Meloni, D., di Sarra, A., DeLuisi, J., Di Iorio, T., Fiocco, G., Junkermann, W., and Pace, G.:  
781 Tropospheric aerosols in the Mediterranean: 2. Radiative effects through model simulations and  
782 measurements, *J. Geophys. Res.*, 108(D10), 4317, doi:10.1029/2002JD002807, 2003.
- 783 Millán, M., Salvador, R., Mantilla, E., and Artinãno, B.: Meteorology and photochemical air  
784 pollution in Southern Europe: experimental results from EC research projects, *Atmos. Environ.*,  
785 30 (12), 1909–1924, 1996.
- 786 Millan, M. M., Salvador, R., Mantilla, E., and Kallos, G.: Photooxidant dynamics in the Western  
787 Mediterranean in summer: Results from European research projects, *J. Geophys. Res.*, 102(D7),  
788 8811–8823, 1997.
- 789 Millán, M. M., Mantilla, E., Salvador, R., Carratala, A., Sanz, M. J., Alonso, L., Gangoiti, G., and  
790 Navazo, M.: Ozone cycles in the western Mediterranean basin: interpretation of monitoring data  
791 in complex terrain, *J. Appl. Meteorol.*, 4, 487–507, 2000.
- 792 Monks, P., Granier, C., Fuzzi, S., Stohl, A., Williams, M., Akimoto, H., Amann, M., Baklanov, A.,  
793 Baltensperger, U., Bey, I., Blake, N., Blake, R., Carslaw, K., Cooper, O., Dentener, F., Fowler,  
794 D., Fragkou, E., Frost, G., Generoso, S., Ginoux, P., Grewe, V., Guenther, A., Hansson, H.,  
795 Henne, S., Hjorth, J., Hofzumahaus, A., Huntrieser, H., Isaksen, I., Jenkin, M., Kaiser, J.,  
796 Kanakidou, M., Klimont, Z., Kulmala, M., Laj, P., Lawrence, M., Lee, J., Liousse, C., Maione,  
797 M., McFiggans, G., Metzger, A., Mieville, A., Moussiopoulos, N., Orlando, J., O’Dowd, C.,  
798 Palmer, P., Parrish, D., Petzold, A., Platt, U., Pöschl, U., Prévôt, A., Reeves, C., Reimann, S.,  
799 Rudich, Y., Sellegri, K., Steinbrecher, R., Simpson, D., ten Brink, H., Theloke, J., van der Werf,  
800 G., Vautard, R., Vestreng, V., Vlachokostas, C., and von Glasow, R.: Atmospheric composition  
801 change – global and regional air quality, *Atmos. Environ.*, 43, 5268–5350,  
802 doi:10.1016/j.atmosenv.2009.08.021, 2009.
- 803 Müller, D., Ansmann, A., Wagner, F., Franke, K., and Althausen, D.: European pollution outbreaks  
804 during ACE 2: Microphysical particle properties and single-scattering albedo inferred from  
805 multiwavelength lidar observations, *J. Geophys. Res.*, 107, D15, 4248, 10.1029/2001JD001110,  
806 2002.
- 807 Nedélec, P., Cammas, J.-P., Thouret, V., Athier, G., Cousin, J.-M., Legrand, C., Abonnel, C.,  
808 Lecoœur, F., Cayez, G., and Marizy, C.: An improved infrared carbon monoxide analyser for  
809 routine measurements aboard commercial Airbus aircraft: technical validation and first scientific  
810 results of the MOZAIC III programme, *Atmos. Chem. Phys.*, 3, 1551–1564, doi:10.5194/acp-3-  
811 1551-2003, 2003.
- 812 Nie, W., Ding, A., Wang, T., Kerminen, V.-M., George, C., Xue, L., Wang, W., Zhang, Q., Petaja,  
813 T., Qi, X., Gao, X., Wang, X., Yang, X., Fu, C., and Kulmala, M.: Polluted dust promotes new  
814 particle formation and growth, *Sci. Rep.*, 4, 6634, doi:10.1038/srep06634, 2014.

815 Nilsson, E. D., Rannik, U., Kulmala, M., Buzorius, G., and, O'Dowd, C. D.: Effects of continental  
816 boundary layer evolution, convection, turbulence and entrainment, on aerosol formation,  
817 *TellusB*, 53, 441–461, 2001.

818 O'Dowd, C., Monahan, C., and Dall'Osto, M.: On the occurrence of open ocean particle production  
819 and growth events, *Geophys. Res. Lett.*, 37, L19805, doi:10.1029/2010GL044679, 2010.

820 Pace, G., di Sarra, A., Meloni, D., Piacentino, S., and Chamard, P.: Aerosol optical properties at  
821 Lampedusa (Central Mediterranean). 1. Influence of transport and identification of different  
822 aerosol types, *Atmos. Chem. Phys.*, 6, 697-713, doi:10.5194/acp-6-697-2006.

823 Pace, G., Junkermann, W., Vitali, L., di Sarra, A., Meloni, D., Cacciani, M., Cremona, G.,  
824 Iannarelli, A. M., and Zanini, G: On the complexity of the boundary layer structure and aerosol  
825 vertical distribution in the coastal Mediterranean regions: a sea breeze, desert dust transport, and  
826 free-tropospheric air intrusion case study in Southern, submitted to *TellusB*, 2015.

827 Parrish, D. D., Holloway, J. S., Trainer, M., Murphy, P. C., Fehsenfeld, F. C., and Forbes, G. L.:  
828 Export of North America ozone pollution to the North Atlantic Ocean, *Science*, 259, 1436–1439,  
829 1993.

830 Parrish, D. D., Trainer, M., Holloway, J. S., Yee, J. E., Warshawsky, M. S., Fehsenfeld, F. C.,  
831 Forbes, G. L., and Moody, J. L.: Relationships between ozone and carbon monoxide at surface  
832 sites in the North Atlantic region, *J. Geophys. Res.*, 103, 13,357– 13,376, 1998.

833 Pérez, C., Sicard, M., Jorba, O., Comeron, A., and Baldasano, J. M.: Summertime re-circulations  
834 of air pollutants over the North-Eastern Iberian coast observed from systematic EARLINET lidar  
835 measurements in Barcelona, *Atmos. Environ.*, 38, 3983–4000, 2004.

836 Pérez, N., Pey, J., Castillo, S., Viana, M., Alastuey, A., and Querol, X.: Interpretation of the  
837 variability of levels of regional background aerosols in the Western Mediterranean, *Sci. Tot.*  
838 *Environ.*, 407, 527–540, 2008.

839 Petzold, A., Fiebig, M., Flentje, H., Keil, A., Leiterer, U., Schroder, F., Stifter, A., Wendisch, M.,  
840 and Wendling, P.: Vertical variability of aerosol properties observed at a continental site during  
841 the Lindenberg Aerosol Characterization Experiment (LACE 98), *J. Geophys. Res.*, 107, 8128,  
842 doi:10.1029/2001JD001043, 2002.

843 Pey, J., Querol, X., and Alastuey, A.: Discriminating the regional and urban contributions in the  
844 North-Western Mediterranean: PM levels and composition, *Atmos Environ*, 44, 1587–96, 2010.

845 Raut, J.-C., and Chazette, P.: Vertical profiles of urban aerosol complex refractive index in the  
846 frame of ESQUIF airborne measurements, *Atmos. Chem. Phys.*, 8, 901–919, 2008.

847 Rose, C., Sellegri, K., Asmi, E., Hervo, M., Freney, E., Junninen, H., Duplissy, J., Sipilä, M.,  
848 Kontkanen, J., Lehtipalo, K., and Kulmala, M.: Major contribution of neutral clusters to new  
849 particle formation in the free troposphere, *Atmos. Chem. Phys. Discuss.*, 14, 18355–18388,  
850 2014.

851 Salameh, T., Drobinski, P., Menut, L., Bessagnet, B., Flamant, C., Hodzic, A., and Vautard, R.:  
852 Aerosol distribution over the western Mediterranean basin during a Tramontane/Mistral event,  
853 *Ann. Geophys.*, 25, 2271–2291, 2007.

854 Sellegri, K., Laj, P., Venzac, H., Boulon, J., Picard, D., Villani, P., Bonasoni, P., Marinoni, A.,  
855 Cristofanelli, P., and Vuillermoz, E.: Seasonal variations of aerosol size distributions based on  
856 long-term measurements at the high altitude Himalayan site of Nepal Climate Observatory-  
857 Pyramid (5079 m), Nepal, *Atmos. Chem. Phys.*, 10, 10679–10690, doi:10.5194/acp-10-10679-  
858 2010, 2010.



859 Soriano, C., Baldasano, J. M., Buttler, W. T., and Moore, K.: Circulatory patterns of air pollutants  
860 within the Barcelona air basin in a summertime situation: lidar and numerical approaches.  
861 *Bound.-Lay. Meteorol.*, 98 (1), 33–55, 2001.

862 Spracklen, D. V., Carslaw, K. S., Kulmala, M., Kerminen, V.-M., Sihto, S.-L., Riipinen, I.,  
863 Merikanto, J., Mann, G. W., Chipperfield, M. P., and Wiedensohler, A.: Contribution of particle  
864 formation to global cloud condensation nuclei concentrations, *Geophys. Res. Lett.*, 35, L06808,  
865 doi:10.1029/2007GL033038, 2008.

866 Stohl, A., Wotawa, G., Seibert, P., and Krompkolb, H.: Interpolation errors in wind fields as a  
867 function of spatial and temporal resolution and their impact on different types of kinematic  
868 trajectories, *J. Appl. Meteorol.*, 34, 2149–2165, 1995.

869 Velchev, K., Cavalli, F., Hjorth, J., Marmer, E., Vignati, E., Dentener, F., and Raes, F.: Ozone over  
870 the Western Mediterranean Sea – results from two years of shipborne measurements, *Atmos.*  
871 *Chem. Phys.*, 11, 675–688, doi:10.5194/acp-11-675-2011, 2011.

872 Wallace J.M., and Hobbs, P.V.: *Atmospheric science: an introductory survey* (2nd edition).  
873 *International Geophysics Series 92*, Academic press, Burlington, 484pp, 2006.

874 Wehner, B., H. Siebert, A. Ansmann, F. Ditas, P. Seifert, F. Stratmann, A. Wiedensohler, A. 956  
875 Apituley, R. A. Shaw, H. E. Manninen, and M. Kulmala (2010), Observations of turbulence  
876 induced new particle formation in the residual layer, *Atmos. Chem. Phys.*, 10, 4319–4330, 958  
877 doi:10.5194/acp-10-4319-2010.

878 Wiegner, M., Emeis, S., Freudenthaler, V., Heese, B., Junkermann, W., Munkel, C., Schäfer, K.,  
879 Seefeldner, M., and Vogt, S.: Mixing layer height over Munich, Germany: variability and  
880 comparisons of different methodologies, *J. Geophys. Res.*, 111, D13201,  
881 doi:10.1029/2005JD006593, 2006.

882 Zhang, L., Jacob, D. J., Bowman, K. W., Logan, J. A., Turquety, S., Hudman, R. C., Li, Q., Beer,  
883 R., Worden, H. M., Worden, J. R., Rinsland, C. P., Kulawik, S. S., Lampel, M. C., Shephard, M.  
884 W., Fisher, B. M., Eldering, A., and Avery M. A.: Ozone-CO correlations determined by the  
885 TES satellite instrument in continental outflow regions, *Geophys. Res. Lett.*, 33, L18804,  
886 doi:10.1029/2006GL026399, 2006.

887

888

889

890



891 **Tables**892 **Table 1.** Summary of information on the TRAQA and SAFMED flights.

893

Measurement campaign	Flight number	Date	Take off-landing time (UTC)	Departure-arrival	Geographic area investigated	Description
TRAQA 2012	V16	20/06/2012	13:12 – 16:34	Toulouse-Toulouse	Gulf of Lion	Test flight
	V17	22/06/2012	09:01 – 12:54	Toulouse-Toulouse	South-western France (over land) and the Atlantic Ocean	Test flight, biogenic emissions
	V18	26/06/2012	07:13 – 09:18	Toulouse-Bastia	Gulf of Genoa	Export of pollution from Northern Italy/Pô Valley, north-westerly winds
	V19	26/06/2012	10:42 – 13:46	Bastia-Toulouse	Gulf of Genoa	Export of pollution from Northern Italy/Pô Valley, north-westerly winds
	V20	27/06/2012	04:07 – 08:00	Toulouse-Nimes	Sea area south of Marseille/Toulon	Export of pollution during a Mistral-Tramontane event
	V21	27/06/2012	09:39 – 13:16	Nimes-Toulouse	Western coast of Corsica	Export of pollution from Northern Italy/Pô Valley, north-westerly winds
	V22	29/06/2012	05:13 – 08:50	Toulouse-Bastia	Eastern coast of Corsica	Dust outbreak
	V23	29/06/2012	10:13 – 14:12	Bastia-Toulouse	Eastern and western coasts of Corsica	Dust outbreak
	V24	03/07/2012	13:19 – 17:12	Toulouse-Toulouse	Sea area north-east of Barcelona	Export of pollution from Barcelona, westerly/south-westerly winds
	V25	04/07/2012	07:18 – 10:54	Toulouse-Toulouse	Sea area south of Marseille/Toulon	Follow of Barcelona pollution plumes
	V26	04/07/2012	15:25 – 18:36	Toulouse-Toulouse	Gulf of Lion	Follow of Barcelona pollution plumes
	V27	06/07/2012	08:00 – 11.55	Toulouse-Toulouse	Sea area south of Marseille	Export of pollution during a moderate Mistral-Tramontane event
	V28	06/07/2012	14:01 – 17:45	Toulouse-Toulouse	Sea area south of Nice/Toulon	Export of pollution during a moderate Mistral-Tramontane event
	V29	07/07/2012	08:19 – 10:59	Toulouse-Nimes	Southern France (over land)	Biogenic emissions
	V30	07/07/2012	13:03 – 17:10	Nimes-Toulouse	Gulf of Genoa	Export of pollution during a moderate Mistral-Tramontane event
	V31	10/07/2012	13:41 – 17:21	Toulouse-Toulouse	Eastern coast of Spain	Characterization of pollution near coastal

						sources
	V32	11/07/2012	11:23 – 14:48	Toulouse-Toulouse	Southeastern coast of France and Gulf of Genoa	Characterization of pollution near coastal sources
SAFMED 2013	V46	24/07/2013	10:34 – 13:06	Genoa-Cagliari	Gulf of Genoa and eastern coast of Corsica and Sardinia	Characterization of pollution plumes in the Gulf of Genoa, Corsica, and Sardinia; westerly/south-westerly winds
	V47	24/07/2013	14:21 – 16:29	Cagliari-Genoa	Eastern coast of Corsica and Sardinia and Gulf of Genoa	Characterization of pollution plumes in the Gulf of Genoa, Corsica, and Sardinia; westerly/south-westerly winds
	V48	25/07/2013	13:12 – 16:02	Genoa-Ersa	Gulf of Genoa	Characterization of pollution in the Gulf of Genoa; westerly/south-westerly winds
	V49	27/07/2013	11:08 – 13:07	Genoa-Alghero	Central Italy (over land)	Characterization of pollution in central Italy
	V50	27/07/2013	15:33 – 16:48	Alghero-Genoa	Eastern coast of Corsica and Gulf of Genoa	Characterization of pollution plumes in the Gulf of Genoa, Corsica, and Sardinia; westerly/south-westerly winds + dust outbreak
	V51	30/07/2013	13:05 – 15:50	Genoa-Ersa	Gulf of Genoa	Characterization of pollution in the Gulf of Genoa; very low north/north-westerly winds
	V52	01/08/2013	12:03 – 15:24	Genoa-Alghero	Western coast of Corsica	Characterization of pollution in western Corsica; export of pollution from Northern Italy/Pô Valley; north-easterly winds

894  
895  
896  
897  
898  
899  
900  
901

902 **Table 2.** Comparison of the number concentrations  $dN_{\text{Aitken}}$  (0.004-0.1  $\mu\text{m}$ ) and  $dN_{\text{Acc}}$  (0.1-1.0  $\mu\text{m}$ )  
 903 observed during the TRAQA/SAFMED field campaigns with those reported in literature for  
 904 continental Europe. All literature data refer to airborne measurements.  
 905

Atmospheric layer	Parameter	TRAQA/SAFMED	Literature over continental Europe
Free troposphere (FT)	$dN_{\text{Aitken}}$ ( $\text{scm}^{-3}$ )	0-19250	812-9149 <sup>b</sup> ; 0-980 <sup>e</sup>
	$dN_{\text{Acc}}$ ( $\text{scm}^{-3}$ )	34-3233	20-80 <sup>a</sup> ; 25-85 <sup>c</sup> ; 0-500 <sup>f</sup>
Boundary layer (BL)	$dN_{\text{Aitken}}$ ( $\text{scm}^{-3}$ )	4-22471	1037-31370 <sup>b</sup> ; 1000-20000 <sup>c</sup> ; 0-30000 <sup>d</sup> ; 0-19000 <sup>e</sup>
	$dN_{\text{Acc}}$ ( $\text{scm}^{-3}$ )	90-3215	70-560 <sup>a</sup> ; 10-50 <sup>c</sup> ; 400-1200 <sup>e</sup> ; 0-2000 <sup>f</sup>

906  
 907 <sup>a</sup> Petzold et al. (2002), Central Europe, July-August 1998; size range  $dN_{\text{Acc}}$  ( $>0.15 \mu\text{m}$ )

908 <sup>b</sup> Mallet et al. (2005), Southeastern France, June 2001; size range  $dN_{\text{Aitken}}$  (0.006-0.6  $\mu\text{m}$ )

909 <sup>c</sup> Wiegner et al. (2006), Germany, May 2003; ; size range  $dN_{\text{Aitken}}$  ( $>0.01 \mu\text{m}$ ),  $dN_{\text{Acc}}$  ( $>0.3 \mu\text{m}$ )

910 <sup>d</sup> Junkermann (2009), Po Valley, July-August 2002 and Septmeber-October 2003; ; size range  $dN_{\text{Aitken}}$  ( $>0.01 \mu\text{m}$ )

911 <sup>e</sup> Hamburger et al. (2012), central Europe, May 2008; size range  $dN_{\text{Aitken}}$  (0.004-0.15  $\mu\text{m}$ ),  $dN_{\text{Acc}}$  ( $>0.15 \mu\text{m}$ )

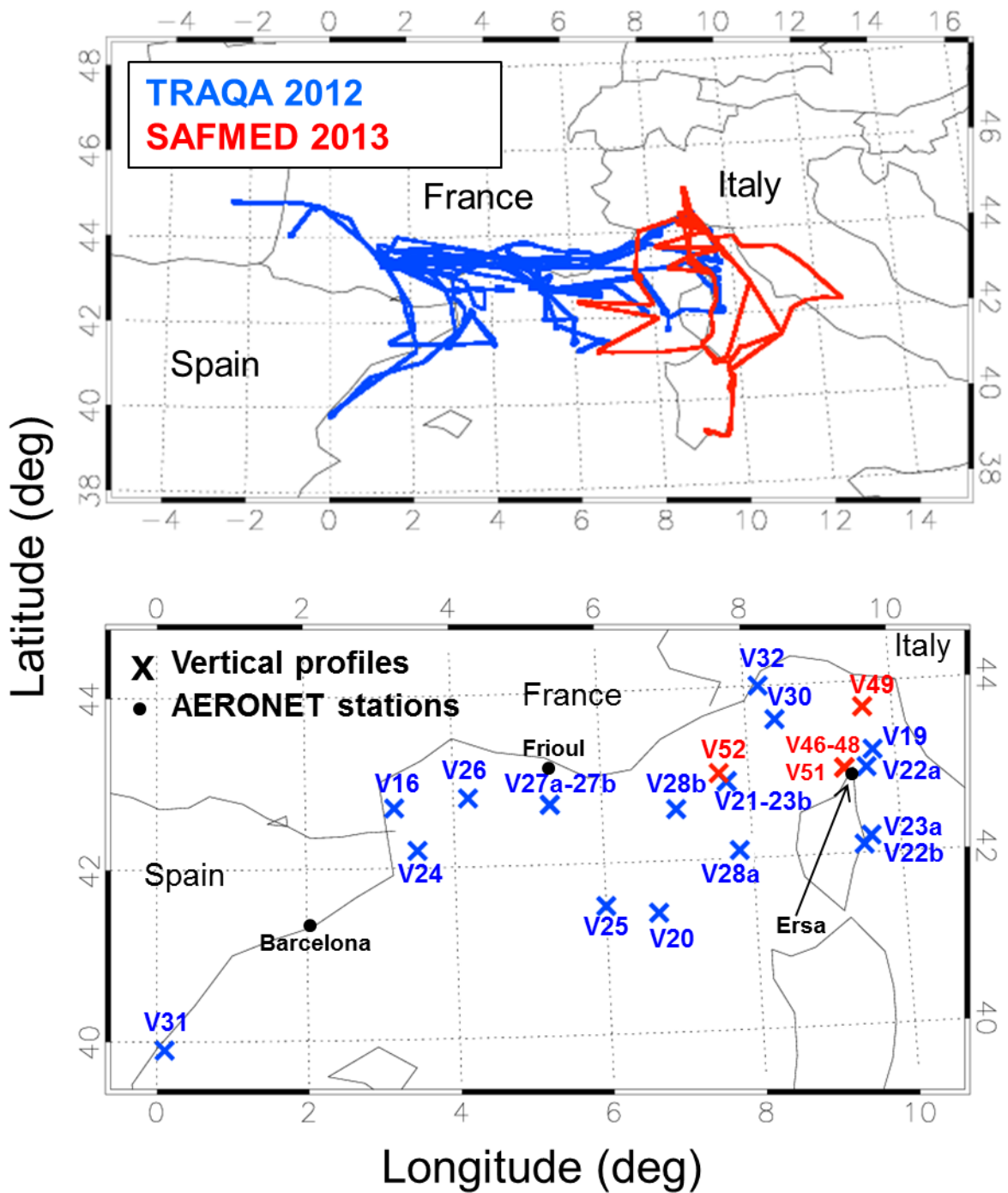
912 <sup>f</sup> Highwood et al. (2012), central Europe, May 2008; size range  $dN_{\text{Aitken}}$  (0.004-0.15  $\mu\text{m}$ ),  $dN_{\text{Acc}}$  ( $>0.15 \mu\text{m}$ )

913  
 914  
 915  
 916  
 917  
 918  
 919  
 920  
 921  
 922  
 923  
 924  
 925  
 926  
 927  
 928  
 929  
 930  
 931  
 932  
 933

934 **Figures**

935 **Figure 1.** (Upper panel) Flight trajectories of the TRAQA (20 June - 13 July 2012) and the  
936 SAFMED (24 July - 1 August 2013) campaigns. The aircraft was based in Toulouse (43°36'N,  
937 1°26'E, France) during TRAQA and in Genoa (44°24'N, 8°55'E, Italy) during SAFMED. (Lower panel)  
938 Zoom on the investigated area and geographical position of the different vertical soundings  
939 analysed in this paper. The position of the three AERONET stations of Barcelona, Frioul, and Ersa  
940 considered in this study is also shown.

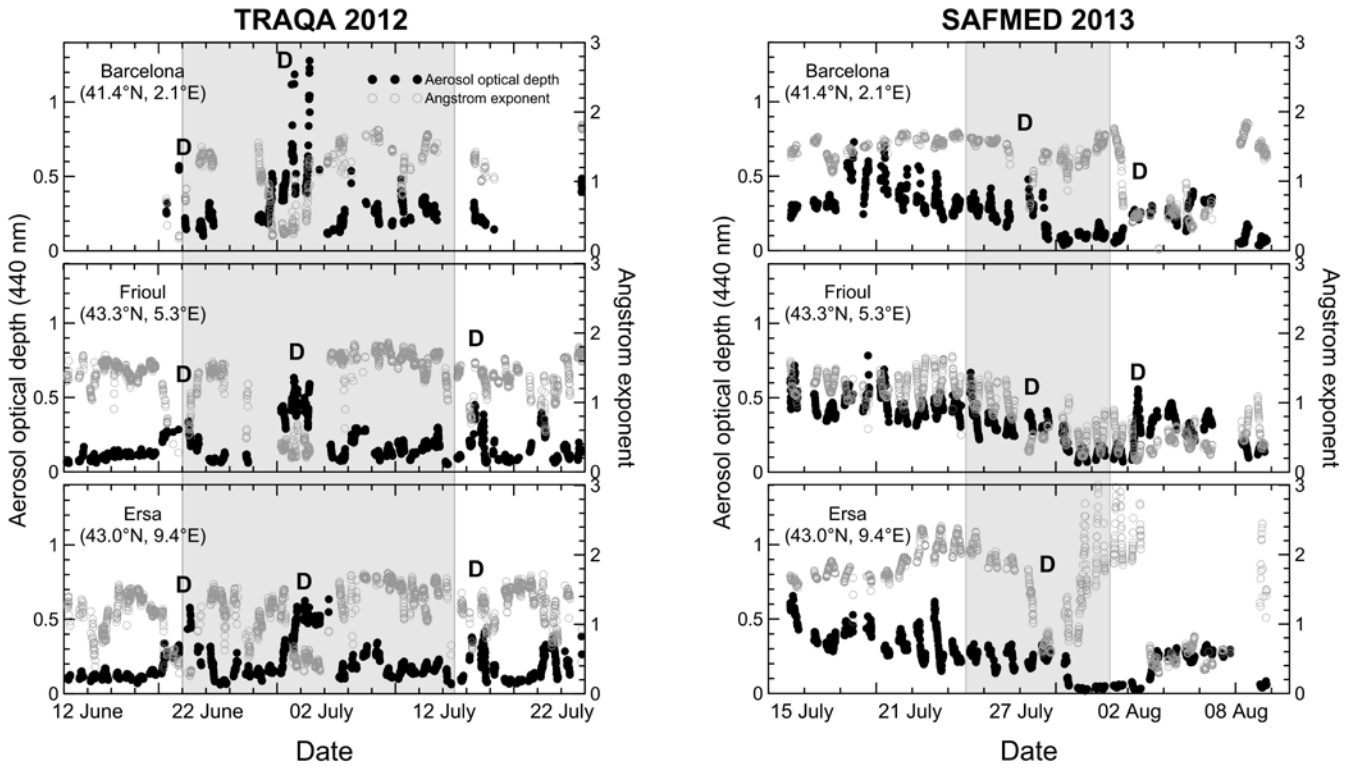
941  
942



943  
944  
945  
946

947 **Figure 2.** Aerosol optical depth at 440 nm ( $\tau$ ) and Ångström exponent ( $\alpha$ ) measured at the  
 948 Barcelona, Frioul, and Ersa AERONET stations during the TRAQA 2012 (left panels) and the  
 949 SAFMED 2013 (right panels) campaigns. The time period for the different plots is  $\pm 10$  days around  
 950 the beginning/end of the two campaigns (data for the Barcelona station are not available over the  
 951 entire period for 2012). The label D indicates the days affected by Saharan dust.  
 952

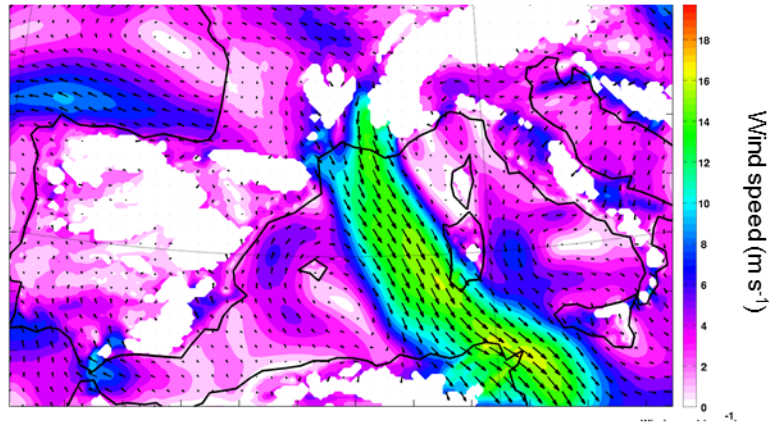
953  
 954



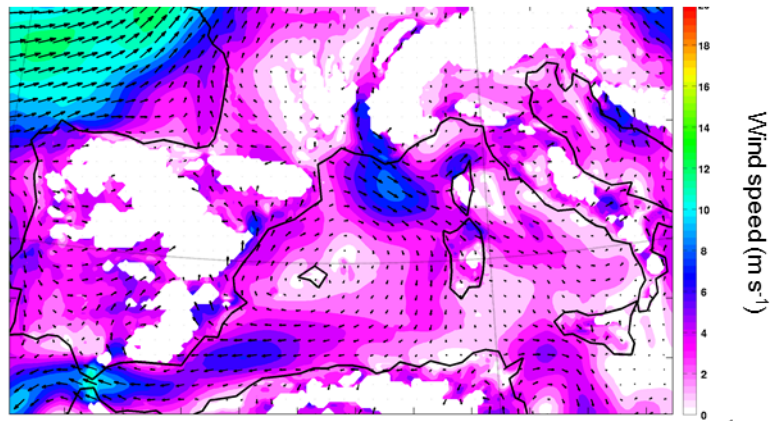
955  
 956  
 957  
 958  
 959  
 960  
 961  
 962  
 963  
 964  
 965  
 966  
 967  
 968  
 969  
 970

971 **Figure 3.** Example of wind maps at 925 mbar for 26 June and 3 July 2012. The maps are obtained  
972 from the WRF-Chem model (Weather Research and Forecasting – Chemistry) at 10-km horizontal  
973 resolution.  
974

a) 26 June 2012 12UT, 925 hPa



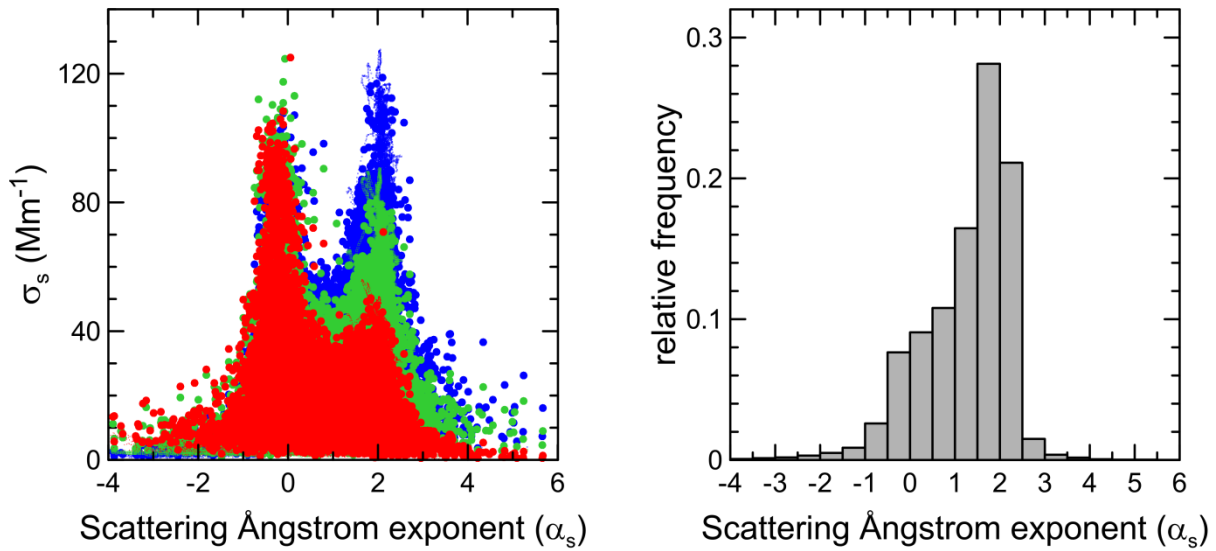
b) 03 July 2012 12UT, 925 hPa



975  
976  
977  
978  
979  
980  
981  
982  
983  
984  
985  
986

987 **Figure 4.** (Left) Scattering coefficient  $\sigma_s$  at 450, 550, and 700 nm versus the scattering Ångstrom  
988 exponent  $\alpha_s$ . Cases with extremely negative ( $<-2$ ) and positive ( $>4$ ) values of  $\alpha_s$  are always related  
989 with very low scattering coefficients, and are likely due to instrumental noise under low scattering  
990 conditions. (Right) Frequency of occurrence of  $\alpha_s$  obtained considering vertical profiles data from  
991 all TRAQA and SAFMED flights.

992



993

994

995

996

997

998

999

1000

1001

1002

1003

1004

1005

1006

1007

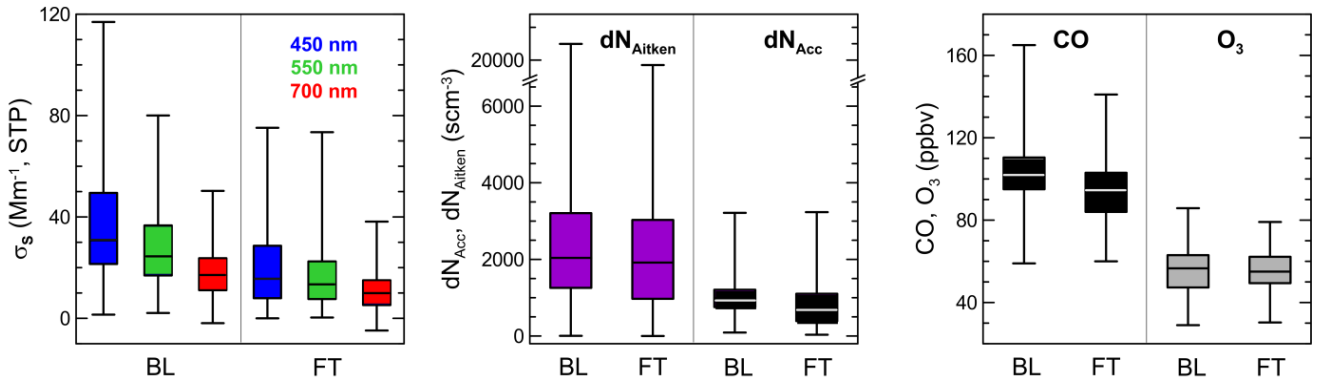
1008

1009

1010

1011

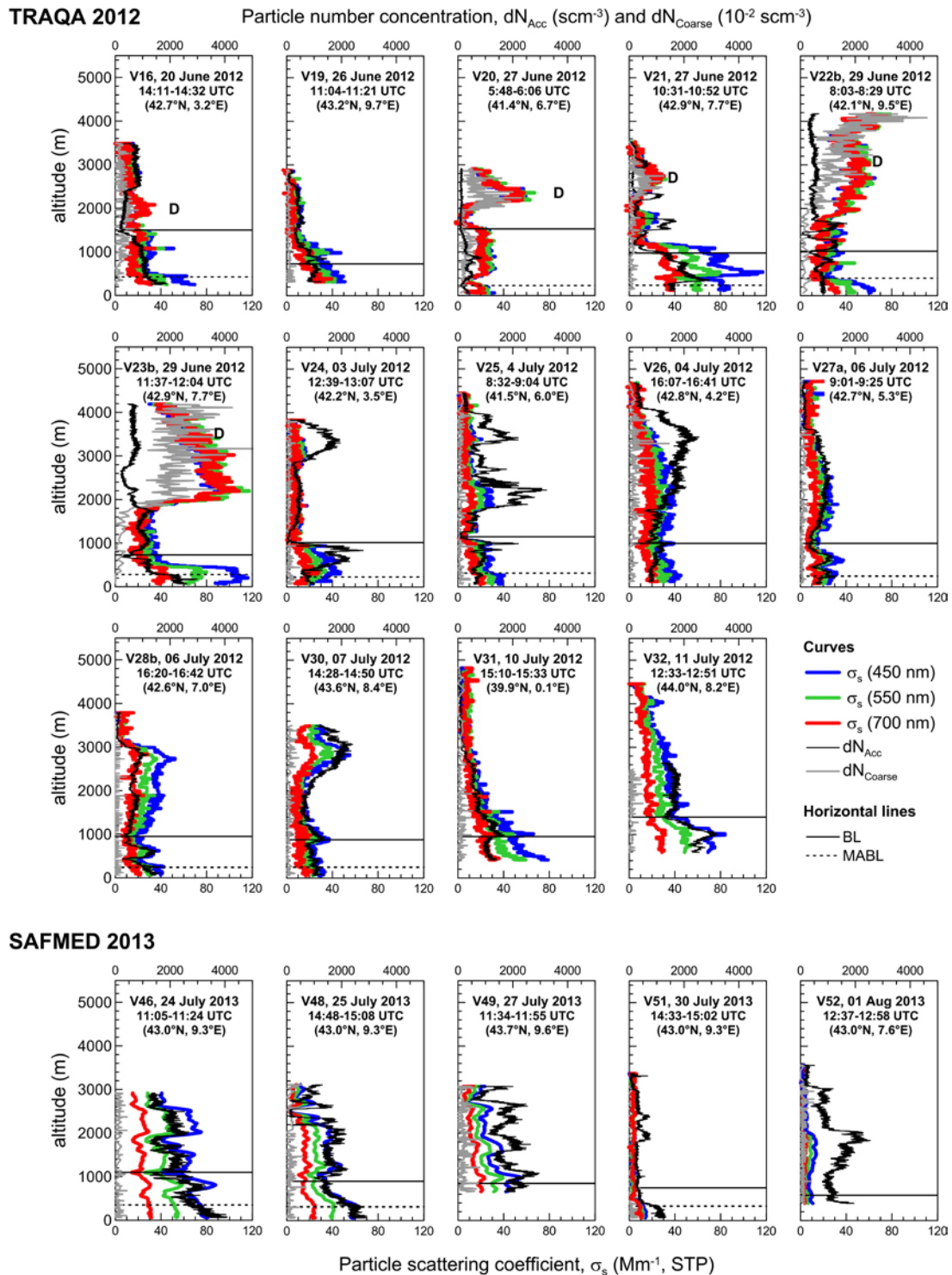
1012 **Figure 5.** Box and whisker plot of the aerosol scattering coefficient ( $\sigma_s$ ) at 450, 550, and 700 nm,  
 1013 particle concentration in the Aitken ( $dN_{\text{Aitken}}$ ) and accumulation ( $dN_{\text{Acc}}$ ) modes, and CO and O<sub>3</sub>  
 1014 measured within pollution plumes in the boundary layer (BL) and in the free troposphere (FT).  
 1015  
 1016



1017  
 1018  
 1019  
 1020  
 1021  
 1022  
 1023  
 1024  
 1025  
 1026  
 1027  
 1028  
 1029  
 1030  
 1031  
 1032  
 1033  
 1034  
 1035  
 1036  
 1037  
 1038  
 1039  
 1040  
 1041  
 1042  
 1043  
 1044  
 1045  
 1046  
 1047  
 1048  
 1049  
 1050  
 1051

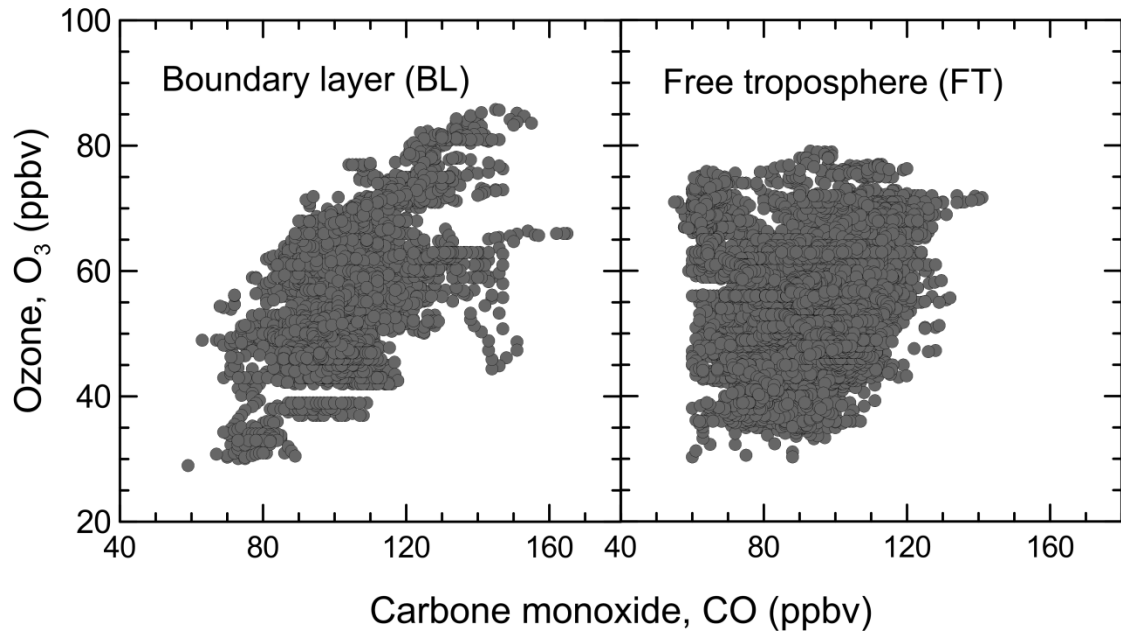


1052 **Figure 6.** Vertical profiles of the spectral scattering coefficient  $\sigma_s$  at 450, 550, and 700 nm and  
 1053 particle number concentration in the 0.1-1.0  $\mu\text{m}$  ( $dN_{\text{Acc}}$ ) and 1.0-4.0  $\mu\text{m}$  ( $dN_{\text{Coarse}}$ ) diameter ranges  
 1054 observed during TRAQA and SAFMED. Data are reported at STP (standard temperature and  
 1055 pressure,  $T = 293.15$  K and  $P = 1013.25$  hPa). The heights of the top of the marine aerosol boundary  
 1056 layer (MABL) and planetary boundary layer (BL) estimated from the meteorological profiles are  
 1057 also indicated in the plots. The label D is used to identify the aerosol layers affected by Saharan  
 1058 dust. For certain flights (V22, V23, V27, and V28) two vertical soundings were performed; the  
 1059 letters “a” and “b” after the flight number in this plot specify if the considered data are taken from  
 1060 the first or the second sounding, respectively.  
 1061



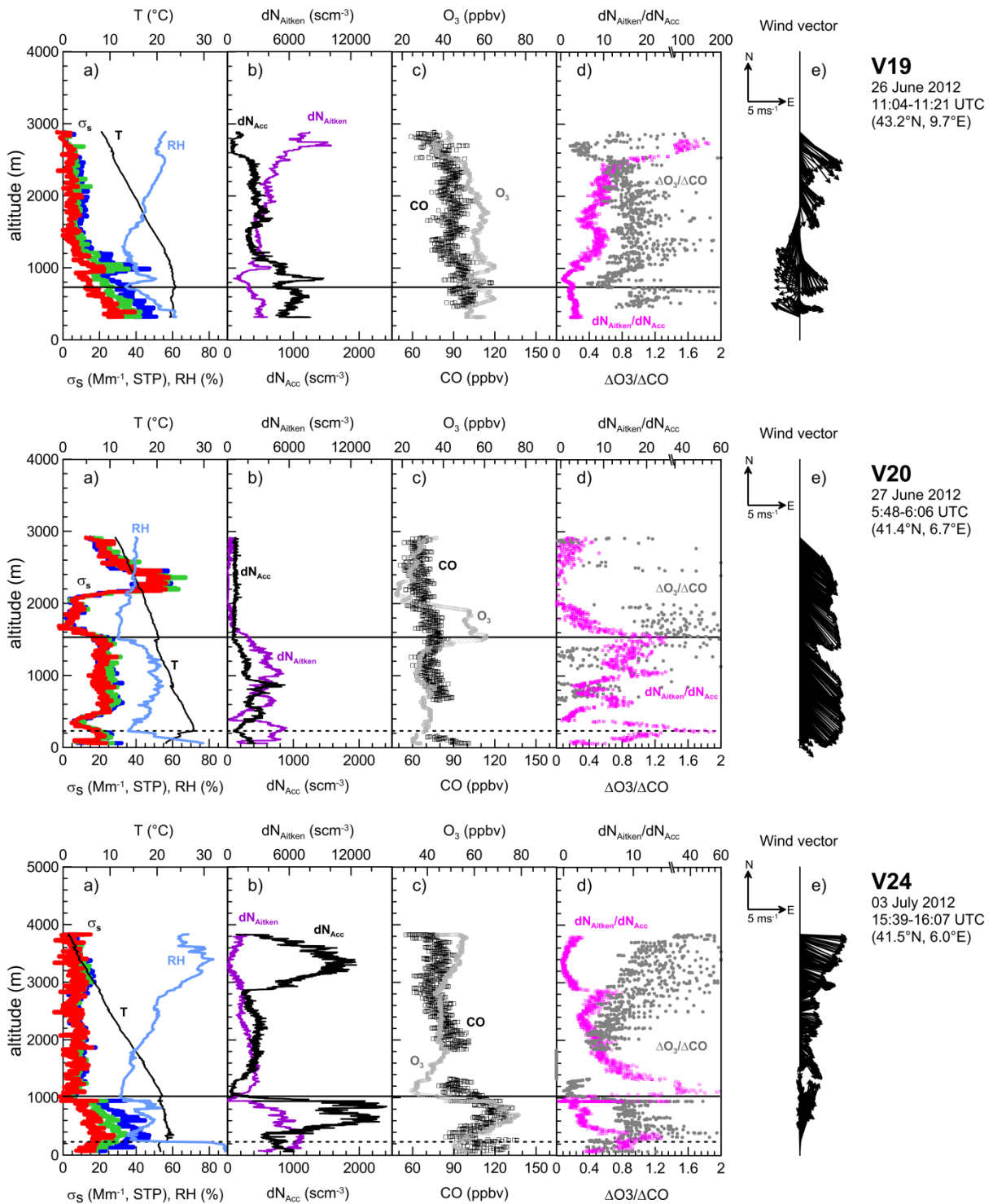
1063  
1064  
1065  
1066  
1067

**Figure 7.** O<sub>3</sub> versus CO in the boundary layer (BL) and the free troposphere (FT) for all TRAQA and SAFMED vertical profiles (dust observations excluded).



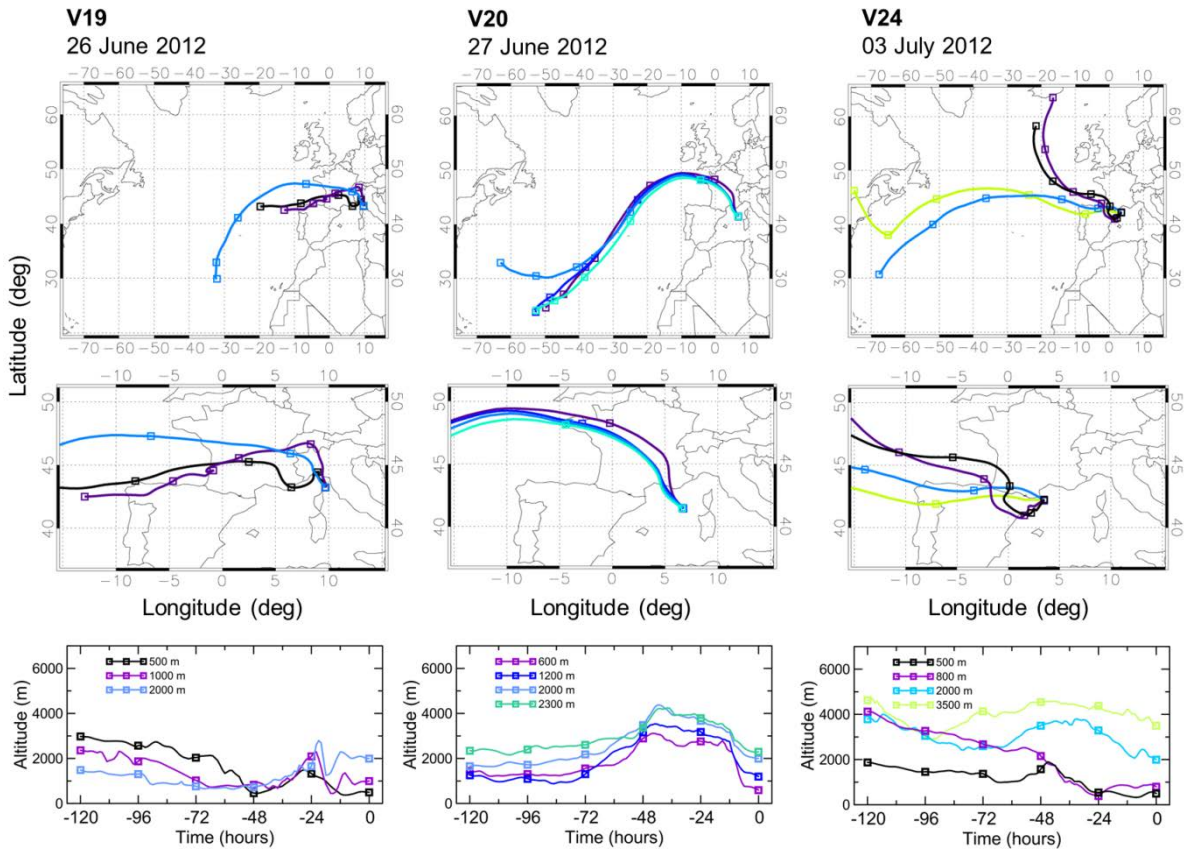
1068  
1069  
1070  
1071  
1072  
1073  
1074  
1075  
1076  
1077  
1078  
1079  
1080  
1081  
1082  
1083  
1084  
1085  
1086  
1087  
1088  
1089  
1090  
1091  
1092  
1093  
1094  
1095  
1096

1097 **Figure 8.** Aerosol and trace gases vertical profiles for flights V19 (export from northern Italy/Po  
 1098 Valley), V20 (Mistral event), and V24 (export from the Barcelona area). The plots show the: (a)  
 1099 spectral scattering coefficient  $\sigma_s$  at 450, 550, and 700 nm (blue, green, and red lines, respectively),  
 1100 temperature (T, black line), and relative humidity (RH, light blue line); (b) particle number  
 1101 concentration in the 0.004-0.1  $\mu\text{m}$  ( $dN_{\text{Aitken}}$ , purple line) and 0.1-1.0  $\mu\text{m}$  ( $dN_{\text{Acc}}$ , black line)  
 1102 diameter ranges, (c) CO (black dots) and O<sub>3</sub> (grey dots) mixing ratios, (d) ozone enhancement factor  
 1103  $\Delta\text{O}_3/\Delta\text{CO}$  (grey dots) and Aitken to accumulation ratio  $dN_{\text{Aitken}}/dN_{\text{Acc}}$  (pink dots) and (e) horizontal  
 1104 wind vector. The heights of the top of the MABL (dotted line) and BL (solid line) are also  
 1105 indicated.  
 1106



1107

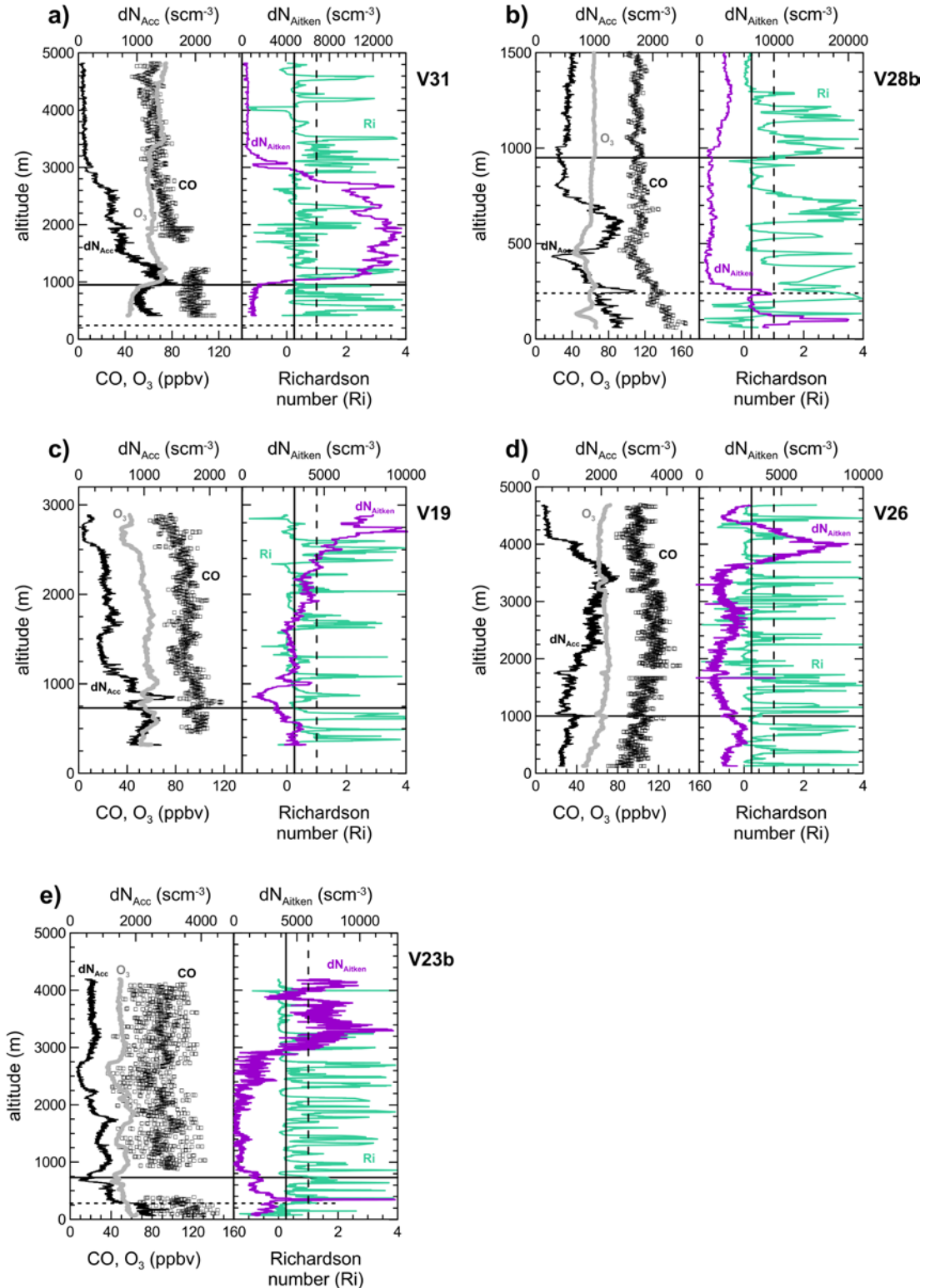
1108 **Figure 9.** Five-days backward air mass trajectories for the V19, V20, and V24 flights calculated  
 1109 with the FLEXTRA model. The upper panel shows the trajectories over an extended latitude-  
 1110 longitude region, while the central panel zooms on the Western Mediterranean area. The altitude of the  
 1111 air masses and its temporal evolution along the five days trajectories is reported in the lower  
 1112 panel of each plot.  
 1113



1114  
 1115  
 1116  
 1117  
 1118  
 1119  
 1120  
 1121  
 1122  
 1123  
 1124  
 1125  
 1126  
 1127

1128  
1129  
1130  
1131  
1132  
1133  
1134

**Figure 10.** Vertical profiles of the accumulation and Aitken particle concentrations ( $dN_{Acc}$ , black line, and  $dN_{Aitken}$ , purple line), CO (black dots), O<sub>3</sub> (grey dots), and gradient Richardson number (Ri, green line) for flights a) V31, b) V28, c) V19, d) V26 and e) V23b. The horizontal lines indicate the height of the marine boundary layer MABL (dotted line) and the planetary boundary layer BL (continuous line), while the vertical lines indicate  $Ri_{crit}=0.25$  and  $Ri=1$  (continuous and dashed lines, respectively).



1135